Computers and Structures 270 (2022) 106814

Contents lists available at ScienceDirect

Computers and Structures

journal homepage: www.elsevier.com/locate/compstruc

Time splitting ratio in the ρ_∞-Bathe time integration method for higher-order accuracy in structural dynamics and heat transfer

Bokyu Choi [a], Klaus-Jürgen Bathe [b], Gunwoo Noh [c,*]

[a] Kyungpook National University, Daegu 41566, Republic of Korea
[b] Massachusetts Institute of Technology, Cambridge, MA 02139, USA
[c] Korea University, Seoul 02841, Republic of Korea

ARTICLE INFO

Article history:
Received 14 January 2022
Accepted 26 April 2022
Available online 15 June 2022

Keywords:
Direct time integrations
Implicit schemes
Bathe method
Order of accuracy
Structural dynamics
Heat transfer

ABSTRACT

Our objective in this paper is to investigate the use of the splitting ratio, γ, in the ρ_∞-Bathe method to reach a higher-order accuracy in the finite element solutions of structural dynamics and heat transfer problems. We study the order of accuracy of the method for both types of analyses, and identify a real-valued γ_p resulting into third-order accuracy with $\rho_\infty = (-1, 1-\sqrt{3}]$ and a complex-valued γ_i with $\rho_\infty \in [0, 1]$ providing at least third-order accuracy but γ_i with $\rho_\infty = 1$ gives fourth-order accuracy. In both types of analyses, structural and heat transfer solutions, the γ values result into the same orders of convergence. To illustrate our theoretical findings, we give the results of some example solutions of structural dynamics and heat flow problems. These solutions show that more accurate response predictions can be obtained when using the more effective γ values.

1. Introduction

The finite element method is widely used to solve various practical engineering problems. For transient analysis, the method of mode superposition can be most effective in some cases. However, direct time integration is commonly used when the response shall be calculated for a relatively short time span, and when a nonlinear response is to be evaluated [1–3]. For direct time integrations, explicit schemes are usually employed when the problem of interest requires a very small time step size for an accurate solution. On the other hand, the use of an unconditionally implicit scheme can be effective.

Various procedures are employed for the solution of the finite element structural dynamic equations [4–10]. In the last decade, following the publication of the standard Bathe method [11,12], a number of research efforts have focused on further investigating existing methods or developing new methods based on the composite strategy with sub-steps, see e.g. [13–23].

Recently, the ρ_∞-Bathe implicit solution scheme was proposed as a generalization of the standard Bathe method to change its spectral properties to reach a more effective scheme [24]. The method was initially introduced as a second-order method, then in later work first- and third-order accurate forms were identified [25,26]. The effective use of the method for wave propagation analysis was also studied [27].

While the time step is divided into two sub-steps in a Bathe method, the scheme is used as a single-step scheme with "internal procedures". All the solution valuables at the intermediate time point, $t + \gamma\Delta t$, are only used to calculate the solutions at the full step [28,29,26]. Therefore, we can consider schemes, to be selected, in which the internal procedures simply calculate certain variables at the intermediate time point, with the only objective to provide good physical and enhanced solutions at the full step.

Recently, in that spirit, we investigated the possibility to select optimal loads at the intermediate time point [26]. In some cases, much enhanced solutions at the full step were obtained by "an optimal modeling" of the external load.

In this paper, we further focus on the use of the time step splitting ratio of the ρ_∞-Bathe method but now focus on the truncation errors achieved when using various splitting values.

While the Bathe methods were proposed for structural dynamics, they may also directly be applied to solve the finite element heat transfer equations. It is therefore of value to consider in this paper the use of the time step splitting ratio in the ρ_∞-Bathe method when employed in the solutions of the equations in structural dynamics and heat transfer.

In Section 2, we first review the second-order accurate ρ_∞-Bathe method for structural dynamics, and then discuss its use for the heat transfer equations. In Section 3, we study truncation

* Corresponding author.
E-mail address: gunwoonoh@korea.ac.kr (G. Noh).

https://doi.org/10.1016/j.compstruc.2022.106814
0045-7949/

errors for the ρ_∞-Bathe method to obtain two useful time step splitting ratios providing higher-order accuracy, a real-valued γ_p and a complex-valued γ_i. The value γ_i may, at present, not be of much practical value but is still of general interest. Section 4 provides some illustrative numerical results obtained with various time step splitting ratios in the solutions of linear and nonlinear problems of structural dynamics and heat transfer.

2. Second-order ρ_∞-Bathe method

This section briefly reviews the second-order ρ_∞-Bathe method for structural dynamics and then introduces its use in the solution of the finite element heat transfer equations.

2.1. Structural dynamics

Considering linear analysis, the governing finite element equations in structural dynamics to be solved are

$$\mathbf{M}\ddot{\mathbf{U}} + \mathbf{C}\dot{\mathbf{U}} + \mathbf{K}\mathbf{U} = \mathbf{R} \tag{1}$$

where $\boldsymbol{M}$, $\boldsymbol{C}$, $\boldsymbol{K}$ are the mass, damping and stiffness matrices, and the vectors $\boldsymbol{U}$ and $\boldsymbol{R}$ list, respectively, the nodal displacements, including rotations, and externally applied nodal forces, including moments. $\dot{\boldsymbol{U}}$ and $\ddot{\boldsymbol{U}}$ are respectively the first and second derivatives of $\boldsymbol{U}$ with respect to time.

In the ρ_∞-Bathe method, we calculate the unknown displacements, velocities, and accelerations by considering the time step Δt to consist of two sub-steps. The sub-step sizes are $\gamma\Delta t$ and $(1-\gamma)\Delta t$ for the first and second sub-steps, respectively, where γ is the time step splitting ratio.

In the first sub-step, we use the trapezoidal rule for the equilibrium at time $t+\gamma\Delta t$,

$$\boldsymbol{M}\,{}^{t+\gamma\Delta t}\ddot{\boldsymbol{U}} + \boldsymbol{C}\,{}^{t+\gamma\Delta t}\dot{\boldsymbol{U}} + \boldsymbol{K}\,{}^{t+\gamma\Delta t}\boldsymbol{U} = {}^{t+\gamma\Delta t}\boldsymbol{R} \tag{2}$$

$${}^{t+\gamma\Delta t}\boldsymbol{U} = {}^{t}\boldsymbol{U} + \frac{\gamma\Delta t}{2}\left({}^{t}\dot{\boldsymbol{U}} + {}^{t+\gamma\Delta t}\dot{\boldsymbol{U}}\right) \tag{3}$$

$${}^{t+\gamma\Delta t}\dot{\boldsymbol{U}} = {}^{t}\dot{\boldsymbol{U}} + \frac{\gamma\Delta t}{2}\left({}^{t}\ddot{\boldsymbol{U}} + {}^{t+\gamma\Delta t}\ddot{\boldsymbol{U}}\right) \tag{4}$$

and in the second sub-step, we use the following relations with the parameters s_0, s_1, s_2, q_0, q_1, q_2, for the equilibrium at time $t+\Delta t$,

$$\boldsymbol{M}\,{}^{t+\Delta t}\ddot{\boldsymbol{U}} + \boldsymbol{C}\,{}^{t+\Delta t}\dot{\boldsymbol{U}} + \boldsymbol{K}\,{}^{t+\Delta t}\boldsymbol{U} = {}^{t+\Delta t}\boldsymbol{R} \tag{5}$$

$${}^{t+\Delta t}\boldsymbol{U} = {}^{t}\boldsymbol{U} + \Delta t\left(q_0\,{}^{t}\dot{\boldsymbol{U}} + q_1\,{}^{t+\gamma\Delta t}\dot{\boldsymbol{U}} + q_2\,{}^{t+\Delta t}\dot{\boldsymbol{U}}\right) \tag{6}$$

$${}^{t+\Delta t}\dot{\boldsymbol{U}} = {}^{t}\dot{\boldsymbol{U}} + \Delta t\left(s_0\,{}^{t}\ddot{\boldsymbol{U}} + s_1\,{}^{t+\gamma\Delta t}\ddot{\boldsymbol{U}} + s_2\,{}^{t+\Delta t}\ddot{\boldsymbol{U}}\right) \tag{7}$$

The Eqs. (2) to (4) and (5) to (7) are in each case three linearly independent equations with three unknowns and can be solved in a variety of ways. We use this procedure:

In the first sub-step, we solve for ${}^{t+\gamma\Delta t}\boldsymbol{U}$ from Eq. (2) by substituting the expressions of ${}^{t+\gamma\Delta t}\dot{\boldsymbol{U}}$ and ${}^{t+\gamma\Delta t}\ddot{\boldsymbol{U}}$ from Eqs. (3) and (4) into Eq. (2), and then calculate ${}^{t+\gamma\Delta t}\dot{\boldsymbol{U}}$ and ${}^{t+\gamma\Delta t}\ddot{\boldsymbol{U}}$. Likewise, in the second sub-step, we obtain ${}^{t+\Delta t}\boldsymbol{U}$ by substituting ${}^{t+\Delta t}\dot{\boldsymbol{U}}$ and ${}^{t+\Delta t}\ddot{\boldsymbol{U}}$ into Eq. (5) and then calculate ${}^{t+\Delta t}\dot{\boldsymbol{U}}$ and ${}^{t+\Delta t}\ddot{\boldsymbol{U}}$ by using Eqs. (6) and (7), respectively.

For the second-order accurate ρ_∞-Bathe method, we use [24]

$$\begin{aligned} q_1 &= s_1 = \tfrac{\rho_\infty+1}{2\gamma(\rho_\infty-1)+4};\\ q_0 &= s_0 = (\gamma-1)q_1 + \tfrac{1}{2};\ \text{and}\ q_2 = s_2 = -\gamma q_1 + \tfrac{1}{2} \end{aligned} \tag{8}$$

With a proper set of values of the parameters, the ρ_∞-Bathe method reduces, as special cases, to the standard scheme, the β_1/β_2-Bathe scheme and the Newmark method at its best use, with $\alpha = 0.25(\delta+0.5)^2$ [14].

Also, the scheme provides the same effective stiffness matrix for each sub-step, with a local maximum of amplitude decay and the global minimum of period elongation [24,25], and the minimum local errors for both the homogeneous and forced responses [26] when using the following value for γ:

$$\gamma_0 = \frac{2-\sqrt{2+2\rho_\infty}}{1-\rho_\infty};\ \ \gamma_0 = 0.5\ \text{ if }\ \rho_\infty = 1 \tag{9}$$

With the above relations, the spectral properties of the second-order accurate ρ_∞-Bathe method can be changed effectively with one parameter, see Ref. [24] where also the step-by-step procedure is summarized. For the selection of the time step sizes Δt in the analysis of structural dynamics and wave propagation problems and the optimal "modeling" of the external load at the sub-step, ${}^{t+\gamma\Delta t}\boldsymbol{R}$ see Refs. [28,29,24,25,27,23,26].

2.2. Heat transfer equations

With the procedures used to analyze structural dynamics problems, we may also calculate the unknown temperature and its time derivative using the second-order ρ_∞-Bathe method in heat transfer analyses. In the first sub-step, we use the trapezoidal rule for the equilibrium at time $t+\gamma\Delta t$

$$\boldsymbol{C}\,{}^{t+\gamma\Delta t}\dot{\boldsymbol{T}} + \boldsymbol{K}\,{}^{t+\gamma\Delta t}\boldsymbol{T} = {}^{t+\gamma\Delta t}\boldsymbol{Q} \tag{10}$$

$${}^{t+\gamma\Delta t}\boldsymbol{T} = {}^{t}\boldsymbol{T} + \frac{\gamma\Delta t}{2}\left({}^{t}\dot{\boldsymbol{T}} + {}^{t+\gamma\Delta t}\dot{\boldsymbol{T}}\right) \tag{11}$$

and in the second sub-step, we consider at time $t+\Delta t$,

$$\boldsymbol{C}\,{}^{t+\Delta t}\dot{\boldsymbol{T}} + \boldsymbol{K}\,{}^{t+\Delta t}\boldsymbol{T} = {}^{t+\Delta t}\boldsymbol{Q} \tag{12}$$

$${}^{t+\Delta t}\boldsymbol{T} = {}^{t}\boldsymbol{T} + \Delta t\left(q_0\dot{\boldsymbol{T}}_t + q_1\,{}^{t+\gamma\Delta t}\dot{\boldsymbol{T}} + q_2\,{}^{t+\Delta t}\dot{\boldsymbol{T}}\right) \tag{13}$$

where $\boldsymbol{C}$ and $\boldsymbol{K}$ are the heat capacity and thermal diffusivity matrices, respectively, $\boldsymbol{Q}$ is the vector of applied nodal heat loads, and $\boldsymbol{T}$ is the vector of nodal temperatures. We use the parameters q_0, q_1, q_2 as determined in Section 2.1, Eq. (8).

With the relations and the equilibrium equations in Eqs. (10)–(13), we can construct the time-stepping equations to solve the heat transfer equations as

$$\hat{\boldsymbol{K}}_1\,{}^{t+\gamma\Delta t}\boldsymbol{T} = \hat{\boldsymbol{Q}}_1 \tag{14}$$

$$\hat{\boldsymbol{K}}_2\,{}^{t+\Delta t}\boldsymbol{T} = \hat{\boldsymbol{Q}}_2 \tag{15}$$

where

$$\hat{\boldsymbol{K}}_1 = \frac{2}{\gamma\Delta t}\boldsymbol{C} + \boldsymbol{K} \tag{16}$$

$$\hat{\boldsymbol{K}}_2 = \frac{2}{q_2\Delta t}\boldsymbol{C} + \boldsymbol{K} \tag{17}$$

$$\hat{\boldsymbol{Q}}_1 = {}^{t+\gamma\Delta t}\boldsymbol{Q} + \boldsymbol{C}\left(\frac{2}{\gamma\Delta t}\,{}^{t}\boldsymbol{T} + {}^{t}\dot{\boldsymbol{T}}\right) \tag{18}$$

$$\hat{\boldsymbol{Q}}_2 = {}^{t+\gamma\Delta t}\boldsymbol{Q} + \boldsymbol{C}\left(\frac{1}{q_2\Delta t}\,{}^{t}\boldsymbol{T} + \frac{1}{q_2}\left(q_0\,{}^{t}\dot{\boldsymbol{T}} + q_1\,{}^{t+\gamma\Delta t}\dot{\boldsymbol{T}}\right)\right) \tag{19}$$

The step-by-step procedure using the ρ_∞-Bathe method for the finite element solution of heat transfer equations is summarized in Table 1 (see Table 2).

Table 1
Step-by-step solution using the ρ_∞-Bathe method for heat equations with general loading.

A. *Initial calculation*
1. Form matrix $\boldsymbol{K}$ and $\boldsymbol{C}$
2. Initialize ${}^0\boldsymbol{T}$ and ${}^0\dot{\boldsymbol{T}}$
3. Select time step Δt, γ, ρ_∞ and calculate integration constants:
   $q_1 = \frac{\rho_\infty+1}{2\gamma(\rho_\infty-1)+4}$; $q_0 = (\gamma-1)q_1 + \frac{1}{2}$; $q_2 = -\gamma q_1 + \frac{1}{2}$
   $a_1 = \frac{2}{\gamma\Delta t}$; $a_3 = \frac{1}{\Delta t q_2}$; $a_7 = \frac{q_0}{q_2}$; $a_8 = \frac{q_1}{q_2}$;
4. Form effective stiffness matrix $\hat{\boldsymbol{K}}_1$ and $\hat{\boldsymbol{K}}_2$:
   $\hat{\boldsymbol{K}}_1 = \boldsymbol{K} + a_1\boldsymbol{C}$; $\hat{\boldsymbol{K}}_2 = \boldsymbol{K} + a_3\boldsymbol{C}$;
5. Triangularize $\hat{\boldsymbol{K}}_1$ and $\hat{\boldsymbol{K}}_2$: $\hat{\boldsymbol{K}}_1 = \boldsymbol{L}_1\boldsymbol{U}_1^{\mathrm{T}}$; $\hat{\boldsymbol{K}}_2 = \boldsymbol{L}_2\boldsymbol{U}_2^{\mathrm{T}}$

B. *For each time step:*
<First sub-step>
1. Calculate effective loads at time $t+\gamma\Delta t$:
   ${}^{t+\gamma\Delta t}\hat{\boldsymbol{R}} = {}^{t+\gamma\Delta t}\boldsymbol{R} + \boldsymbol{C}({}^t\dot{\boldsymbol{T}} + a_1\,{}^t\boldsymbol{T})$
2. Solve for temperatures at time $t+\gamma\Delta t$:
   $\boldsymbol{L}_1\boldsymbol{U}_1^{\mathrm{T}}\,{}^{t+\gamma\Delta t}\boldsymbol{T} = {}^{t+\gamma\Delta t}\hat{\boldsymbol{R}}$
3. Calculate for time $t+\gamma\Delta t$:
   ${}^{t+\gamma\Delta t}\dot{\boldsymbol{T}} = a_1({}^{t+\gamma\Delta t}\boldsymbol{T} - {}^t\boldsymbol{T}) - {}^t\dot{\boldsymbol{T}}$

<Second sub-step>
1. Calculate effective loads at time $t+\Delta t$:
   ${}^{t+\Delta t}\hat{\boldsymbol{R}} = {}^{t+\Delta t}\boldsymbol{R} + \boldsymbol{C}(a_3\,{}^t\boldsymbol{T} + a_7\,{}^t\dot{\boldsymbol{T}} + a_8\,{}^{t+\gamma\Delta t}\dot{\boldsymbol{T}})$
2. Solve for temperatures at time $t+\Delta t$:
   $\boldsymbol{L}_2\boldsymbol{U}_2^{\mathrm{T}}\,{}^{t+\Delta t}\boldsymbol{T} = {}^{t+\Delta t}\hat{\boldsymbol{R}}$
3. Calculate for time $t+\Delta t$:
   ${}^{t+\Delta t}\dot{\boldsymbol{T}} = -a_3\,{}^t\boldsymbol{T} + a_3\,{}^{t+\Delta t}\boldsymbol{T} - a_7\,{}^t\dot{\boldsymbol{T}} - a_8\,{}^{t+\gamma\Delta t}\dot{\boldsymbol{T}}$

3. Higher-order ρ_∞-Bathe method

In this section, we revisit the ρ_∞-Bathe method to identify time step splitting ratios providing higher-order accuracy. With the general form of the ρ_∞-Bathe method, Eqs. (1)–(7), and the relations between the parameters in Eqs. (8) and (9), we revisit the use of γ and the corresponding ρ_∞. We first consider the case of structural dynamics and then the case of heat transfer.

3.1. Structural dynamics

To assess the order of accuracy of the ρ_∞-Bathe method, we use the exact amplification matrix $\boldsymbol{A}_{\text{exact}}$ considering the analytical solution of a typical modal equation, ${}^t\ddot{x} + 2\xi\omega\,{}^t\dot{x} + \omega^2\,{}^t x = 0$. The exact solution of the modal equation without load can be written as

$$\begin{bmatrix} {}^{t+\Delta t}\dot{x} \\ {}^{t+\Delta t}x \end{bmatrix} = \boldsymbol{A}_{\text{exact}} \begin{bmatrix} {}^t\dot{x} \\ {}^t x \end{bmatrix} \tag{20}$$

where

$$\boldsymbol{A}_{\text{exact}} = \begin{bmatrix} \frac{1}{\omega_d}e^{-\xi\omega\Delta t}(-\xi\omega\sin(\omega_d\Delta t) + \omega_d\cos(\omega_d\Delta t)) & -\frac{\xi^2\omega^2+\omega_d^2}{\omega_d}e^{-\xi\omega\Delta t}\sin(\omega_d\Delta t) \\ \frac{1}{\omega_d}e^{-\xi\omega\Delta t}\sin(\omega_d\Delta t) & e^{-\xi\omega\Delta t}\left(\cos(\omega_d\Delta t) + \frac{\xi\omega}{\omega_d}\sin(\omega_d\Delta t)\right) \end{bmatrix} \tag{21}$$

and ω is the natural frequency and $\omega_d = \omega\sqrt{1-\xi^2}$ is the damped natural frequency, and $\Omega = \omega\Delta t$, respectively.

With Eqs. (2)–(7), we form the corresponding numerical amplification matrix $\boldsymbol{A}_{\text{numerical}}$ as (see Appendix)

$$\boldsymbol{A}_{\text{numerical}} = \frac{1}{\beta_1}\begin{bmatrix} a_{11} & a_{12} \\ a_{21} & a_{22} \end{bmatrix} \tag{22}$$

Using Eqs. (21) and (22) for each of the elements in the matrices, we obtain local errors in the ρ_∞-Bathe method

$$\begin{aligned} &\boldsymbol{A}_{\text{exact}}(1,1) - \boldsymbol{A}_{\text{numerical}}(1,1) \\ &= \left(\frac{\xi(2\xi^2-1)(3(\rho_\infty+1)\gamma^2 - 2(\rho_\infty+2)\gamma + 2)}{6 + 3(\rho_\infty-1)\gamma}\right)\Omega^3 \\ &- \left(\frac{(4\xi^2-2\xi-1)(4\xi^2+2\xi-1)(3(\rho_\infty^2-1)\gamma^4 - (\rho_\infty(\rho_\infty-8)-17)\gamma^2 - 4(\rho_\infty+5)\gamma + 8)}{24(2+\gamma(\rho_\infty-1))^2}\right)\Omega^4 + O(\Omega^5) \end{aligned} \tag{23}$$

Table 2
The values of γ and the corresponding ρ_∞ in the ρ_∞-Bathe time integration scheme for structural dynamics and heat flow problems; PE: period elongations, AD: amplitude decays, E_c: error constant.

1. γ_0 in Eq. (9) and $\rho_\infty \in [0,1]$
   (1) Second-order accuracy, Real-valued, Full range of $|\rho_\infty|$
   (2) As $|\rho_\infty|$ decreases, PE, AD and E_c increase
   (3) $\rho_\infty = 0$ is recommended when a general structure is considered in both structural dynamics and heat flow problems

2. γ_p in Eq. (28) with the negative sign and $\rho_\infty \in (-1, 1-\sqrt{3}]$
   (1) Third-order accuracy, Real-valued, Limited range of $|\rho_\infty|$
   (2) As $|\rho_\infty|$ decreases, PE, AD (at $\Delta t << T$) and E_c decrease
   (3) $\rho_\infty = 1-\sqrt{3}$ is always recommended

3. γ_i in Eq. (29) with the negative sign and $\rho_\infty \in [0,1]$
   (1) Third- or fourth-order accuracy ($\rho_\infty \neq 1$ or $\rho_\infty = 1$, respectively), complex-valued, full range of $|\rho_\infty|$
   (2) As $|\rho_\infty|$ decreases, PE, AD and E_c increase
   (3) $\rho_\infty = 0$ is recommended when a general structure is considered in both structural dynamics and heat flow problems
   (4) Use of γ_i may be considered when a small time step size is needed, e.g., when the highest significant frequency contained in the external loads is large

$$\boldsymbol{A}_{\text{exact}}(1,2)-\boldsymbol{A}_{\text{numerical}}(1,2)=\omega\left(\frac{(2\xi-1)(2\xi+1)(3(\rho_\infty+1)\gamma^2-2\rho_\infty\gamma-4\gamma+2)}{24+12(\rho_\infty-1)\gamma}\right)\Omega^3 - \omega\left(\frac{\xi(2\xi^2-1)(3(\rho_\infty^2-1)\gamma^4-(\rho_\infty(\rho_\infty-8)-17)\gamma^2-4(\rho_\infty+5)\gamma+8)}{6(2+(\rho_\infty-1)\gamma)^2}\right)\Omega^4+O(\Omega^5) \tag{24}$$

$$\boldsymbol{A}_{\text{exact}}(2,1)-\boldsymbol{A}_{\text{numerical}}(2,1)=-\frac{1}{\omega}\left(\frac{(2\xi-1)(2\xi+1)(3(\rho_\infty+1)\gamma^2-2\rho_\infty\gamma-4\gamma+2)}{24+12(\rho_\infty-1)\gamma}\right)\Omega^3 + \frac{1}{\omega}\left(\frac{\xi(2\xi^2-1)(3(\rho_\infty^2-1)\gamma^4-(\rho_\infty(\rho_\infty-8)-17)\gamma^2-4(\rho_\infty+5)\gamma+8)}{6(2+(\rho_\infty-1)\gamma)^2}\right)\Omega^4+O(\Omega^5) \tag{25}$$

$$\boldsymbol{A}_{\text{exact}}(2,2)-\boldsymbol{A}_{\text{numerical}}(2,2)=-\left(\frac{\xi(3(\rho_\infty+1)\gamma^2-2(\rho_\infty+2)\gamma+2)}{12+6(\rho_\infty-1)\gamma}\right)\Omega^3 + \left(\frac{(2\xi-1)(2\xi+1)(3(\rho_\infty^2-1)\gamma^4-(\rho_\infty(\rho_\infty-8)-17)\gamma^2-4(\rho_\infty+5)\gamma+8)}{24(2+\gamma(\rho_\infty-1))^2}\right)\Omega^4+O(\Omega^5) \tag{26}$$

Eqs. (23)–(26) show that the ρ_∞-Bathe method is at least $O(\Omega^3)$ in the local truncation error for any γ and ρ_∞; therefore, the scheme gives (globally) second-order accuracy in the numerical solution.

Using the condition for the leading $O(\Omega^3)$ terms in Eqs. (23)–(26) to be zero, we obtain a globally third-order accurate method

$$\rho_\infty=\frac{3\gamma^2-4\gamma+2}{\gamma(2-3\gamma)} \tag{27}$$

With Eq. (27), we find that γ is a real number, $\gamma_{p1,2}$, for $\rho_\infty\in(-1,1-\sqrt{3}]$, and a complex number, $\gamma_{i1,2}$, for $\rho_\infty\in(1-\sqrt{3},1]$

$$\gamma_{p1,2}=\frac{\rho_\infty+2\pm\sqrt{\rho_\infty^2-2\rho_\infty-2}}{3(\rho_\infty+1)};\qquad \rho_\infty\in(-1,1-\sqrt{3}] \tag{28}$$

$$\gamma_{i1,2}=\frac{\rho_\infty+2\pm\sqrt{\rho_\infty^2-2\rho_\infty-2}}{3(\rho_\infty+1)};\qquad \rho_\infty\in(1-\sqrt{3},1] \tag{29}$$

where the subscripts 1 and 2 correspond to the positive and negative signs, respectively. Note that $\rho_\infty=-1$ provides $\gamma=1$ in Eq. (27), and a zero denominator in the parameters defined in Eq. (8); hence we do not use $\rho_\infty=-1$.

We also note that with $\gamma_{i1,2}$ in Eq. (29) and $\rho_\infty=1.0$, the terms corresponding to $O(\Omega^4)$ in Eqs. (23)–(26) are all eliminated: hence, the ρ_∞-Bathe method with $\gamma_{i1,2}$ and $\rho_\infty=1.0$ has a global fourth-order accuracy with and without physical damping.

While the $\gamma_{p1,2}$ provide identical spectral properties with and without damping, their values are quite different for a given ρ_∞. Fig. 1 shows the values of $\gamma_{p1,2}$ and $\gamma_{i1,2}$ in their corresponding ρ_∞ ranges. Since the $\gamma_{p1,2}$ are real numbers, there are no imaginary parts. The values of $\gamma_{p2}\in(1,1+\frac{\sqrt{3}}{3}]$ are more favorable than those of $\gamma_{p1}\in[1+\frac{\sqrt{3}}{3},\infty)$. Therefore, we only consider γ_{p2} as γ_p for the real-valued γ resulting into a third-order accurate ρ_∞-Bathe method. Note that γ_{p2} is identical to the γ value derived from the period elongations and amplitude decays [25] and was shown to minimize errors in forced and homogeneous responses in the third-order ρ_∞-Bathe method [26].

As with the values $\gamma_{p1,2}$, the complex γ values, $\gamma_{i1,2}$, provide identical spectral properties, i.e., identical numerical amplification matrices $\boldsymbol{A}_{\text{numerical}}$. Also, considering $\rho_\infty\in(1-\sqrt{3},1]$, we have $Re(\gamma_{i1,2})\in(1+\frac{\sqrt{3}}{3},\frac{1}{2}]$, and $Im(\gamma_{i1})\in(0,\frac{\sqrt{3}}{3}]$ and $Im(\gamma_{i2})\in[-\frac{\sqrt{3}}{3},0)$. We use γ_{i2} as γ_i for the complex γ providing third-order accuracy with $\rho_\infty\in(1-\sqrt{3},1)$ and fourth-order accuracy with $\rho_\infty=1$.

Note that with γ_i, we have complex solution variables at the intermediate time point; however, we always have real solution variables at the full step for all $\rho_\infty\in[0,1]$. While theoretically interesting, the practical value of using the complex-valued γ_i is probably limited in current computing environments but we give some solutions in Section 4. These promising solutions suggest that the most effective use of γ_i in practice should be studied with an optimized solver and optimized memory employed.

Figs. 2 and 3 show the spectral radii of the ρ_∞-Bathe method for various values of ρ_∞ using γ_0 and γ_p or γ_i, respectively. With the γ_0 and γ_i values, the amount of numerical dissipation can be controlled continuously from the non-dissipative case to the asymptotically annihilating case. On the other hand, the use of γ_p results in a limited range of spectral radii at very large time step size, namely $[-1+\sqrt{3},1)$ due to its applicable range of $\rho_\infty\in(-1,1-\sqrt{3}]$.

As shown in the amplitude decay and period elongation curves of γ_p and γ_0 in Fig. 4 for all $\rho_\infty\in(-1,1-\sqrt{3}]$, γ_p gives a more significant increase in errors than using γ_0. However, the third-order accuracy renders γ_p useful in some analyses as we shall see in Section 4.

Fig. 5 shows the amplitude decays and the period elongations of the ρ_∞-Bathe method with γ_i and γ_0. The use of γ_i with positive ρ_∞ values gives less period elongations but larger amplitude decays compared to the use of γ_0 for the complete range of $\Delta t/T_0$. Also, the use of γ_i with negative $\rho_\infty\in(1-\sqrt{3},0)$ provides larger amplitude decays and period elongations than γ_i with positive ρ_∞ values of the same $|\rho_\infty|$. Therefore, in structural analysis, we consider γ_i with $\rho_\infty\in[0,\ 1]$.

In Fig. 6, we consider a four times larger time step size for the case of γ_i to compare the amplitude decay and period elongation with using γ_0. Considering the required computational cost and the resulting order of accuracy of the method, the use of γ_i may be attractive in some analyses.

3.2. Heat transfer equations

To investigate the numerical characteristics of the ρ_∞-Bathe method in heat transfer solutions, we consider a typical modal equation, $\dot\theta+k\theta=0$, where θ and $\dot\theta$ are the temperature and its time derivative, and k is the thermal diffusivity. The exact solution of this modal equation may be expressed in the form

$$\begin{bmatrix}{}^{t+\Delta t}\dot\theta\\ {}^{t+\Delta t}\theta\end{bmatrix}=\boldsymbol{A}_{\text{exact}}\begin{bmatrix}{}^{t}\dot\theta\\ {}^{t}\theta\end{bmatrix} \tag{30}$$

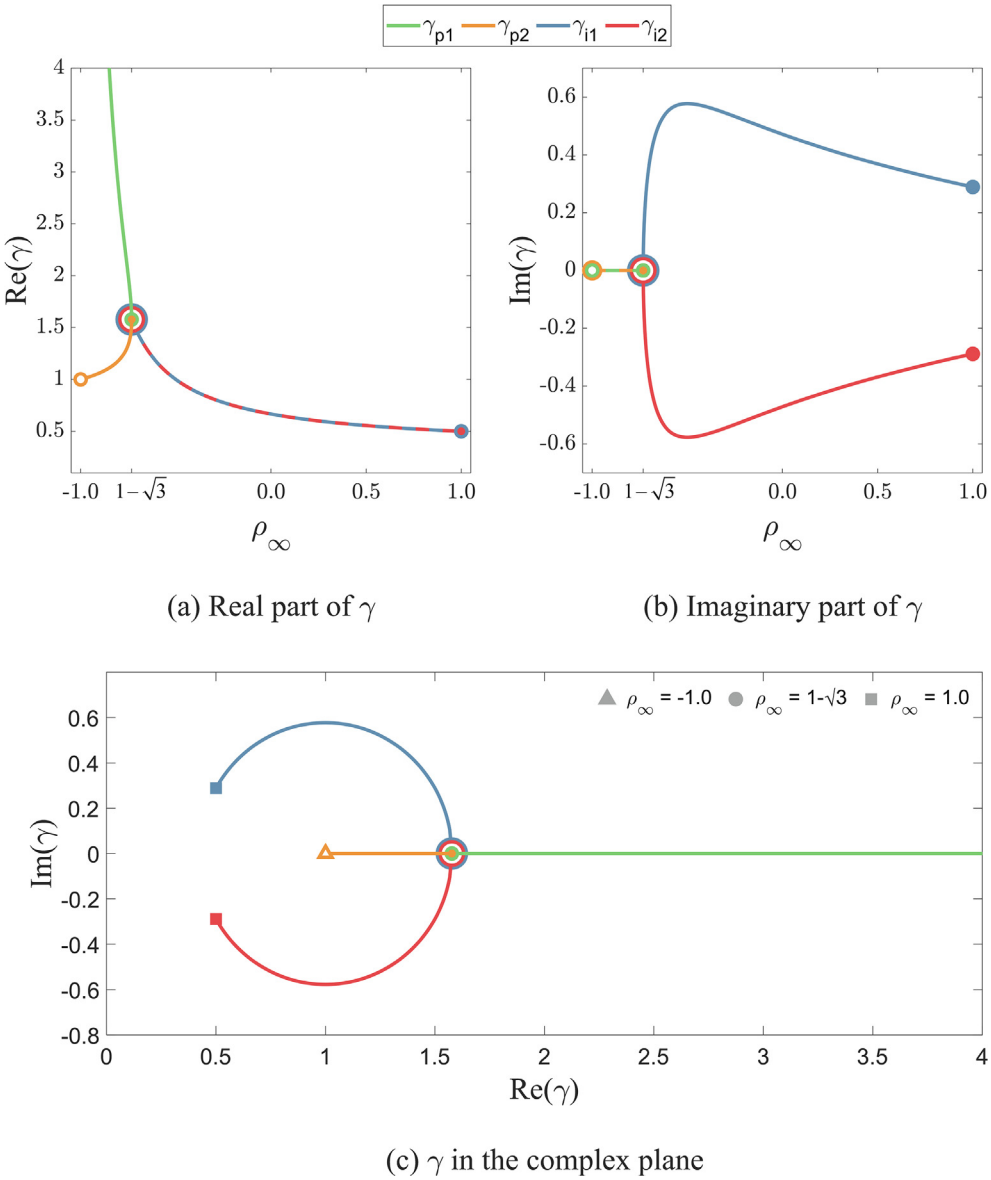

Fig. 1. The real and imaginary parts of $\gamma_{p1,2}$, $\gamma_{i1,2}$, respectively. The imaginary part of $\gamma_{p1,2}$ is always zero ($Im(\gamma_{p1,2}) = 0$).

where

$$\boldsymbol{A}_{\text{exact}} = \begin{bmatrix} e^{-k\Delta t} & 0 \\ 0 & e^{-k\Delta t} \end{bmatrix} \tag{31}$$

and the root of the characteristic polynomial of the matrix $\boldsymbol{A}_{\text{exact}}$ is

$$\lambda_{\text{exact}} = e^{-k\Delta t} \tag{32}$$

With Eqs. (10)–(13), we obtain the corresponding numerical amplification matrix $\boldsymbol{A}_{\text{numerical}}$ as

$$\boldsymbol{A}_{\text{numerical}} = \frac{1}{\kappa}\begin{bmatrix} a_{11} & a_{12} \\ a_{21} & a_{22} \end{bmatrix} \tag{33}$$

where

$$\kappa = ((k\Delta t)\gamma + 2)(((k\Delta t) - \rho_\infty + 1)\gamma - (k\Delta t) - 2) \tag{34}$$

$$a_{11} = (k\Delta t)(\rho_\infty\gamma^2(k\Delta t) + (-\rho_\infty(k\Delta t) + 2\rho_\infty)\gamma - \rho_\infty + 1) \tag{35}$$

$$a_{12} = ((\rho_\infty - 1)\gamma^2(k\Delta t) + (2(k\Delta t) + 2\rho_\infty - 2)\gamma + 4 - (\rho_\infty + 1)(k\Delta t))k \tag{36}$$

$$a_{21} = -\left(\rho_\infty\gamma^2(k\Delta t) + (-\rho_\infty(k\Delta t) + 2\rho_\infty)\gamma - \rho_\infty + 1\right)\Delta t \tag{37}$$

$$a_{22} = -(\rho_\infty - 1)\gamma^2(k\Delta t) + (-2(k\Delta t) - 2\rho_\infty + 2)\gamma - 4 + (\rho_\infty + 1)(k\Delta t) \tag{38}$$

The root of the characteristic polynomial of $\boldsymbol{A}_{\text{numerical}}$ is

$$\lambda_{\text{numerical}} = \frac{(\rho_\infty(k\Delta t) - \rho_\infty + 1)\gamma^2(k\Delta t) + \left(\rho_\infty(k\Delta t)^2 - 2(k\Delta t - 1)(\rho_\infty - 1)\right)\gamma - 2(k\Delta t) + 4}{(\gamma(k\Delta t) + 2)(((k\Delta t) - \rho_\infty + 1)\gamma - (k\Delta t) - 2)} \tag{39}$$

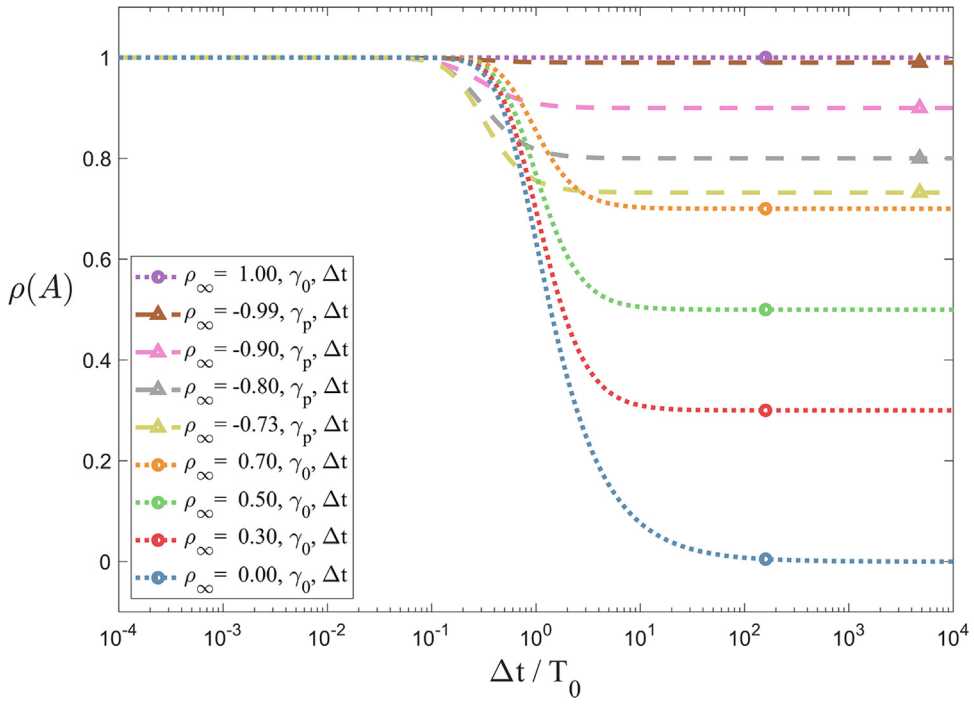

Fig. 2. Spectral radii of approximation operator of the ρ_∞-Bathe method for structural dynamics ($\xi = 0$) for various values of ρ_∞ with γ_0 and γ_p.

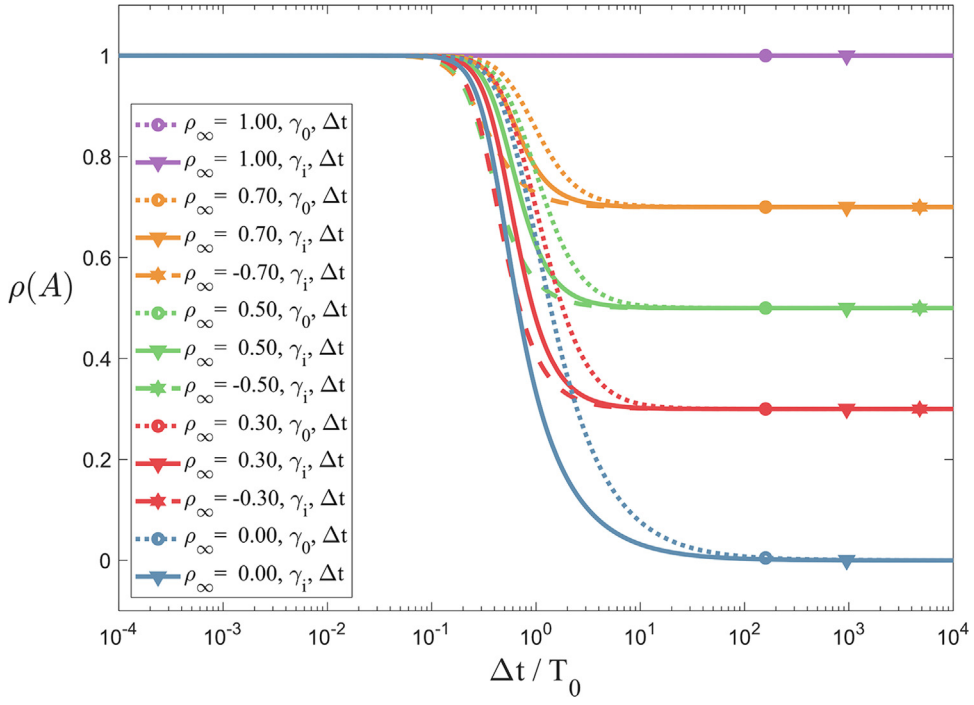

Fig. 3. Spectral radii of approximation operator of the ρ_∞-Bathe method for structural dynamics ($\xi = 0$) for various values of ρ_∞ with γ_0 and γ_i.

Hence we obtain an expression of the local error of $\lambda_{\text{numerical}}$

$$\lambda_{\text{exact}} - \lambda_{\text{numerical}} = -\frac{2-2\gamma(\rho_\infty+2)+3\gamma^2(\rho_\infty+1)}{24+12(\rho_\infty-1)\gamma}(k\Delta t)^3 + \frac{(-3\rho_\infty^2+3)\gamma^4+(\rho_\infty^2-8\rho_\infty-17)\gamma^2+4(\rho_\infty+5)\gamma-8}{24(2+\gamma(\rho_\infty-1))^2}(k\Delta t)^4 + O((k\Delta t)^5) \quad (40)$$

Eq. (40) shows that the local error of the solutions from the ρ_∞ - Bathe method in heat transfer problems is $O((k\Delta t)^3)$; therefore, the method is at least second-order accurate in the solutions of the heat transfer equations, as in structural dynamics.

Since the coefficient of the leading $O((k\Delta t)^3)$ term in Eq. (40) is identical to the coefficients of the leading terms of Eqs. (23)–(26) in the case of $\xi = 0$, we use γ_0 defined in Eq. (9) to minimize the error of the second-order ρ_∞-Bathe method also for heat transfer solu-

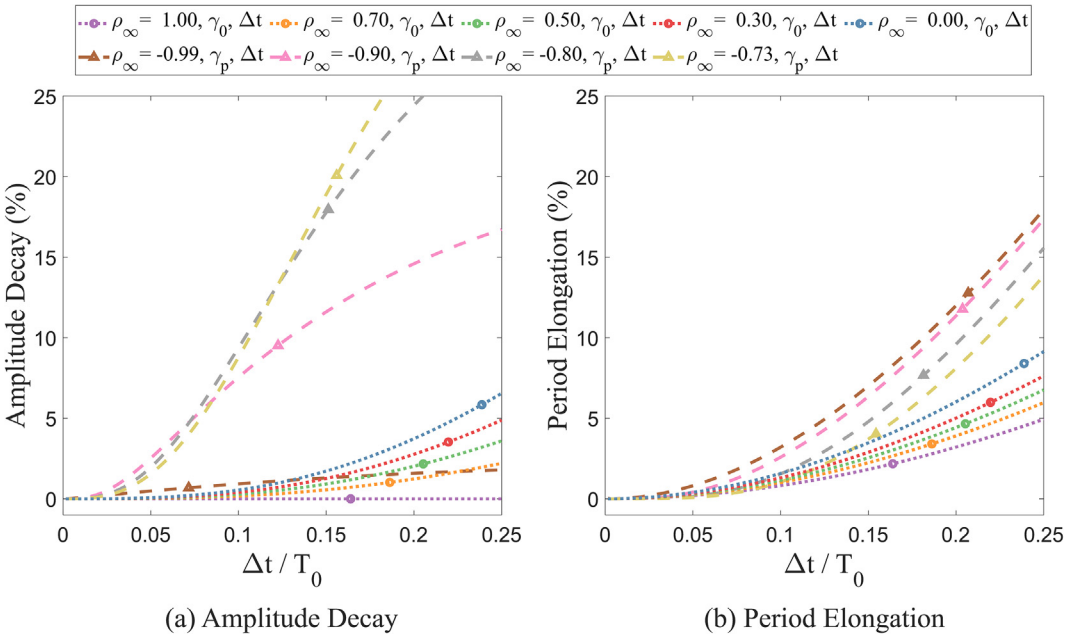

Fig. 4. Amplitude decay and period elongation using the ρ_∞-Bathe method with γ_0 and γ_p in structural dynamics.

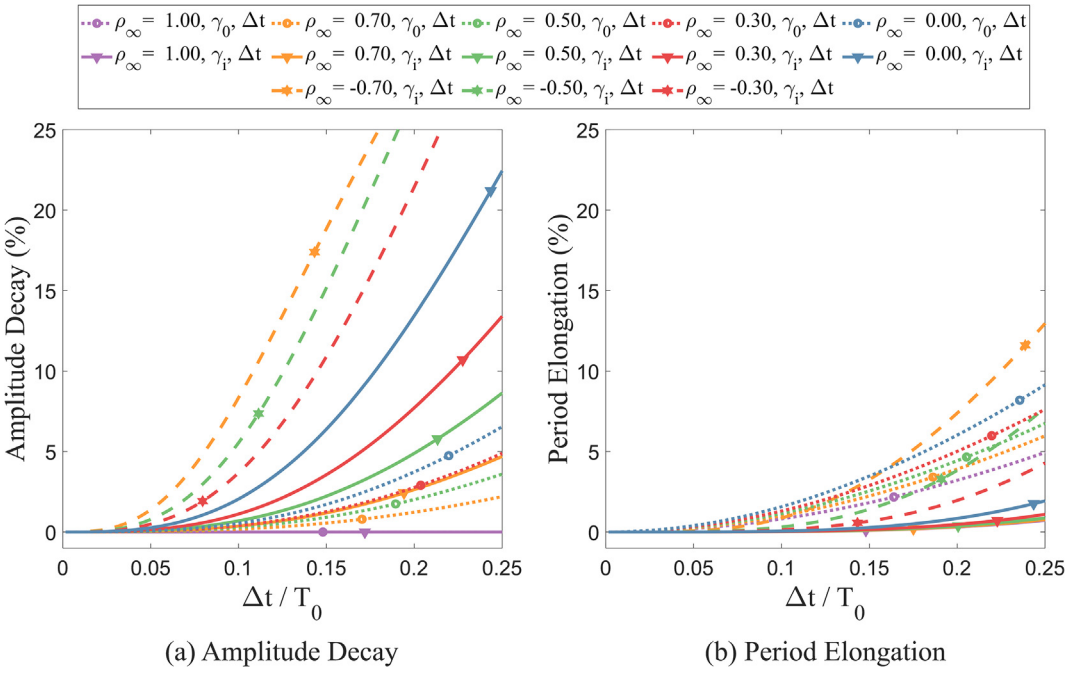

Fig. 5. Amplitude decay and period elongation using the ρ_∞-Bathe method with γ_0 and γ_i in structural dynamics.

tions. We also can use γ_p in $\rho_\infty \in (-1, 1-\sqrt{3}]$ and γ_i in $\rho_\infty \in (1-\sqrt{3}, 1]$ to eliminate the $O\left((k\Delta t)^3\right)$ term for the heat transfer equations.

With γ_i and $\rho_\infty = 1.0$, the error $(\lambda_{\text{exact}} - \lambda_{\text{numerical}})$ is given by

$$\lambda_{\text{exact}} - \lambda_{\text{numerical}} = \frac{1}{720}(k\Delta t)^5 + O\left((k\Delta t)^6\right) \tag{41}$$

Therefore, γ_i with $\rho_\infty = 1.0$ provides fourth-order accuracy also in the solution of the heat transfer equations.

Figs. 7 and 8 show the spectral radii of the ρ_∞-Bathe method for various values of ρ_∞ with γ_0, γ_p and γ_i. The use of γ_0, γ_p and γ_i provides unconditional stability and controllable numerical dissipation. Fig. 9 shows the error constant, $E_c(\gamma, (k\Delta t)^n)$, that is, the coefficient of the leading term of the local error, $O((k\Delta t)^n)$, obtained with γ and $\rho_\infty \in [-1, 1]$.

In the error constant E_c of the ρ_∞-Bathe method with γ_0, the coefficient of the term of $O((k\Delta t)^3)$ is

$$E_c(\gamma_0, (k\Delta t)^3) = \frac{2 - 2\gamma(\rho_\infty + 2) + 3\gamma^2(\rho_\infty + 1)}{24 + 12(\rho_\infty - 1)\gamma} \tag{42}$$

and the error constant E_c of the ρ_∞-Bathe method with γ_p and γ_i of $O((k\Delta t)^4)$ is

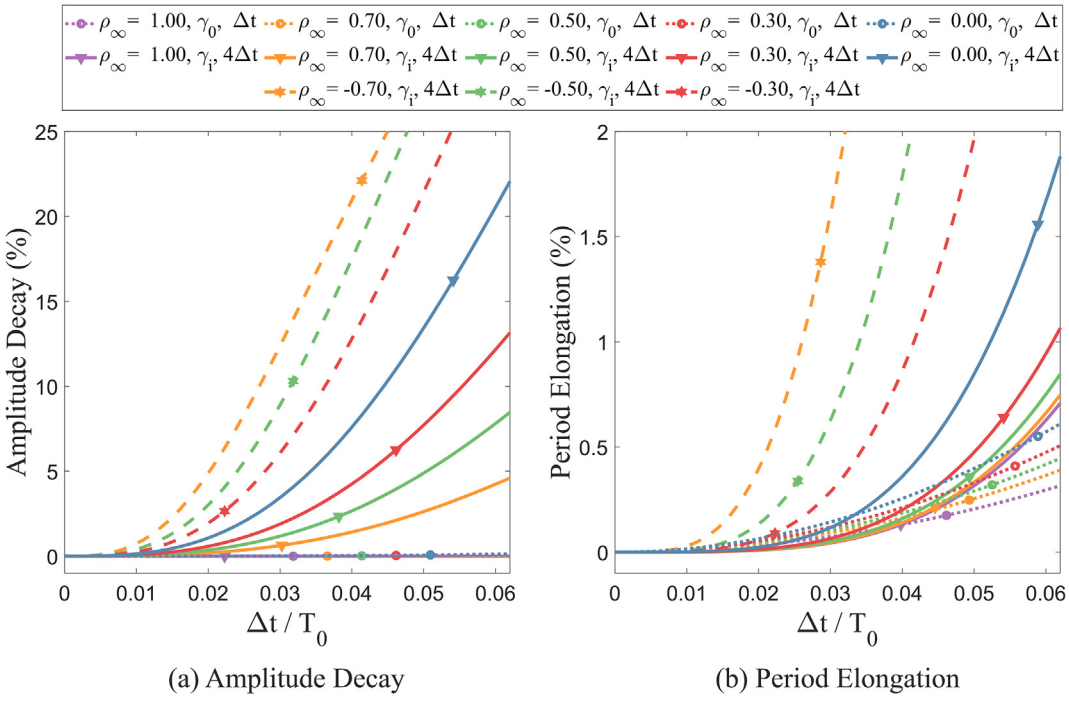

Fig. 6. Amplitude decay and period elongation using the ρ_∞-Bathe method with γ_0 and γ_i in structural dynamics.

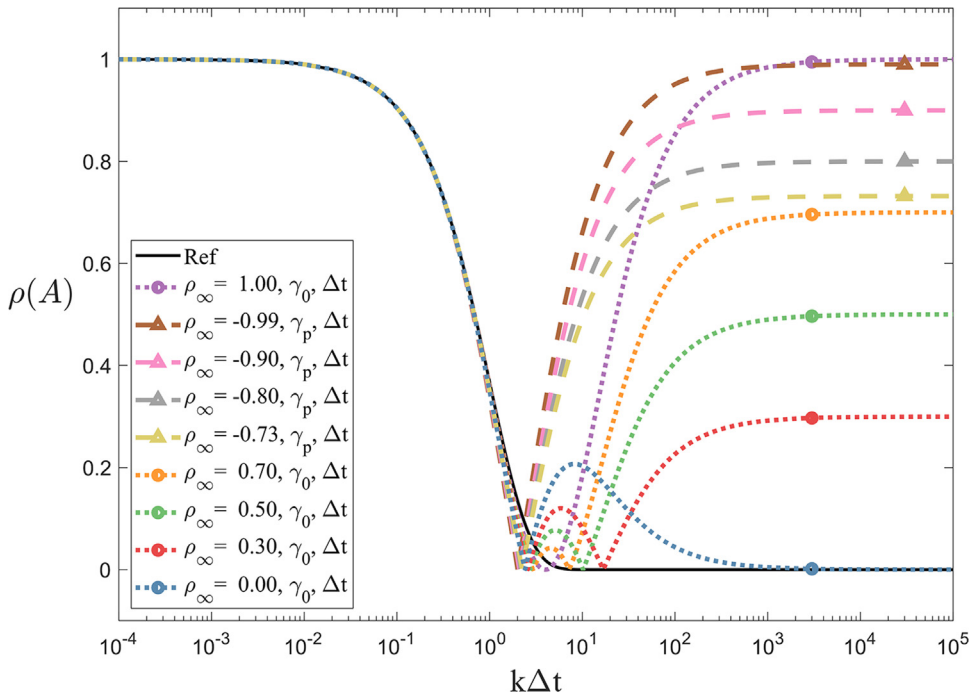

Fig. 7. Spectral radii of approximation operator of the ρ_∞-Bathe method in heat transfer for various values of ρ_∞ with γ_0 and γ_p.

$$E_c(\gamma_{p,i},(k\Delta t)^4) = -\frac{(\rho_\infty-1)\left((-\rho_\infty^3-6\rho_\infty^2+3\rho_\infty+4)\Lambda+\rho_\infty^4+5\rho_\infty^3+30\rho_\infty^2+29\rho_\infty+7\right)}{36(\rho_\infty+1)\left((1-\rho_\infty)\Lambda+\rho_\infty^2+7\rho_\infty+4\right)^2} \tag{43}$$

where

$$\Lambda = \sqrt{\rho_\infty^2-2\rho_\infty-2} \tag{44}$$

For γ_0, γ_p and γ_i, the magnitude of the error constant decreases as the value of ρ_∞ increases from -1 to 1. As the method has fourth-order accuracy with γ_i and $\rho_\infty = 1.0$, we have $E_c(\gamma_i,(k\Delta t)^4) = 0$ at $\rho_\infty = 1$.

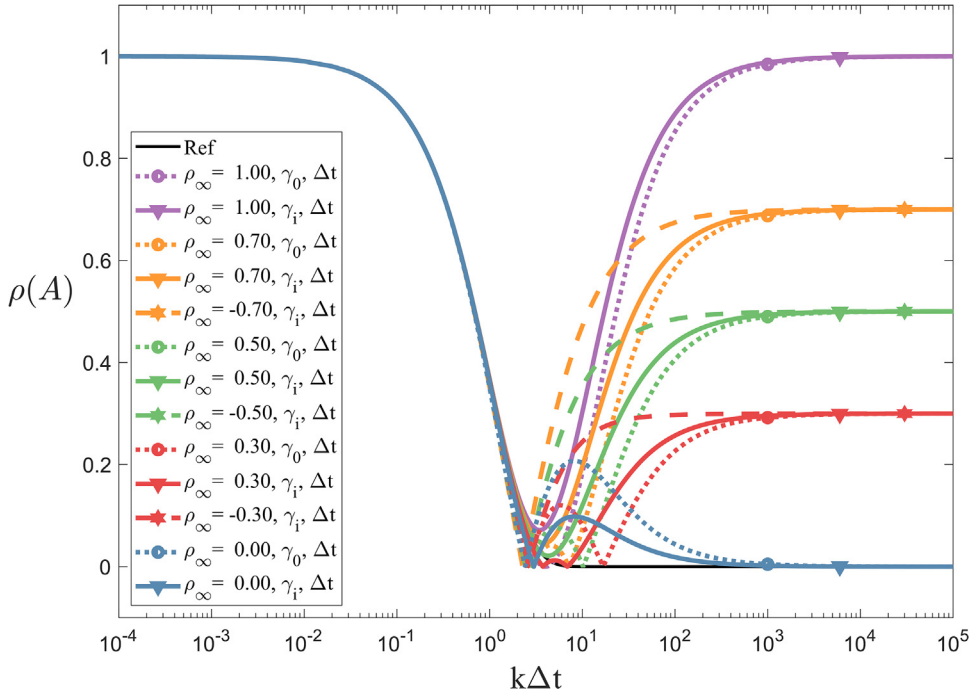

Fig. 8. Spectral radii of approximation operator of the ρ_∞-Bathe method in heat transfer for various values of ρ_∞ with γ_0 and γ_i.

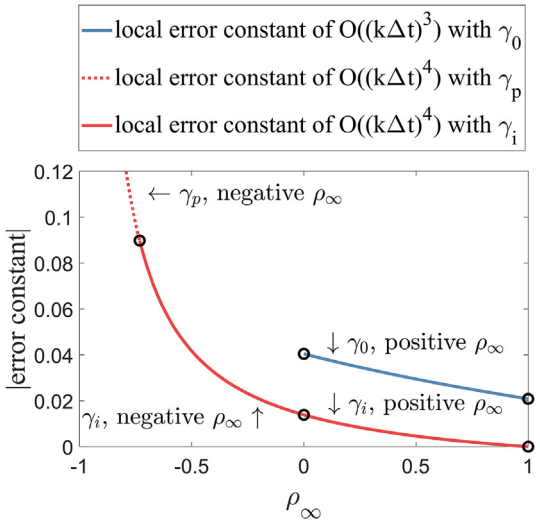

Fig. 9. Error constant of the ρ_∞-Bathe method with γ_0 of $O(k\Delta t^3)$ and with γ_p and γ_i of $O(k\Delta t^4)$, respectively.

As in structural dynamics, the use of γ_i with negative $\rho_\infty \in (1-\sqrt{3}, 0)$ has less favorable characteristics than the use of γ_i with positive $\rho_\infty \in [0, 1]$ since it provides a larger error constant. Therefore, also in heat transfer analyses, we use γ_i only with $\rho_\infty \in [0, 1]$, but again the use of complex arithmetic is for now probably limited in practical analyses.

An important difference to the use of implicit time integration in structural dynamics is that in heat transfer analysis we do not measure period elongations and amplitude decays, but only the rate of convergence, see above. In structural dynamics it can be of crucial importance to *numerically* damp out high spurious frequencies merely introduced because the mesh only represents frequencies accurately up to a certain frequency and higher thus spurious frequencies may introduce large errors in the solution. In heat transfer analysis using some schemes, also unwanted oscillations are introduced for too large time steps used but these are of much less detriment, because heat transfer problems contain always actual physical damping (see Section 4.4).

4. Illustrative numerical results

We solve several linear and nonlinear structural dynamics and heat transfer model problems to illustrate the properties of the ρ_∞-Bathe method with γ_0, γ_p and γ_i. In the numerical examples, we use a four times larger time step size for γ_i since some higher computational cost per step is present.

4.1. A linear damped single-degree-of-freedom system (SDOF)

We consider a damped SDOF system with mass $m = 1$, damping $c = 10$, stiffness $k = 100$, external force $f = \sin(2t)$. To investigate the convergence behavior of the ρ_∞-Bathe method with γ_0, γ_p and γ_i in the displacement, velocity, and acceleration, we use the error norms

$$\text{Error} = \sqrt{\sum_{i=0}^{N} [x_i - x(t_i)]^2 / \sum_{i=0}^{N} x(t_i)^2} \tag{45}$$

where x_i is the exact solution, $x(t_i)$ is the numerical solution at the time t_i, and N is the number of total time steps.

Fig. 10 shows the error norms of displacement, velocity, and acceleration of the ρ_∞-Bathe method with γ_0, γ_p and γ_i at similar computational costs. As we expected in Section 3.1, γ_0 and γ_p provide second- and third-order accuracy, respectively, and γ_i provides third- and fourth-order accuracy for $\rho_\infty \neq 1$ and $= 1$, respectively.

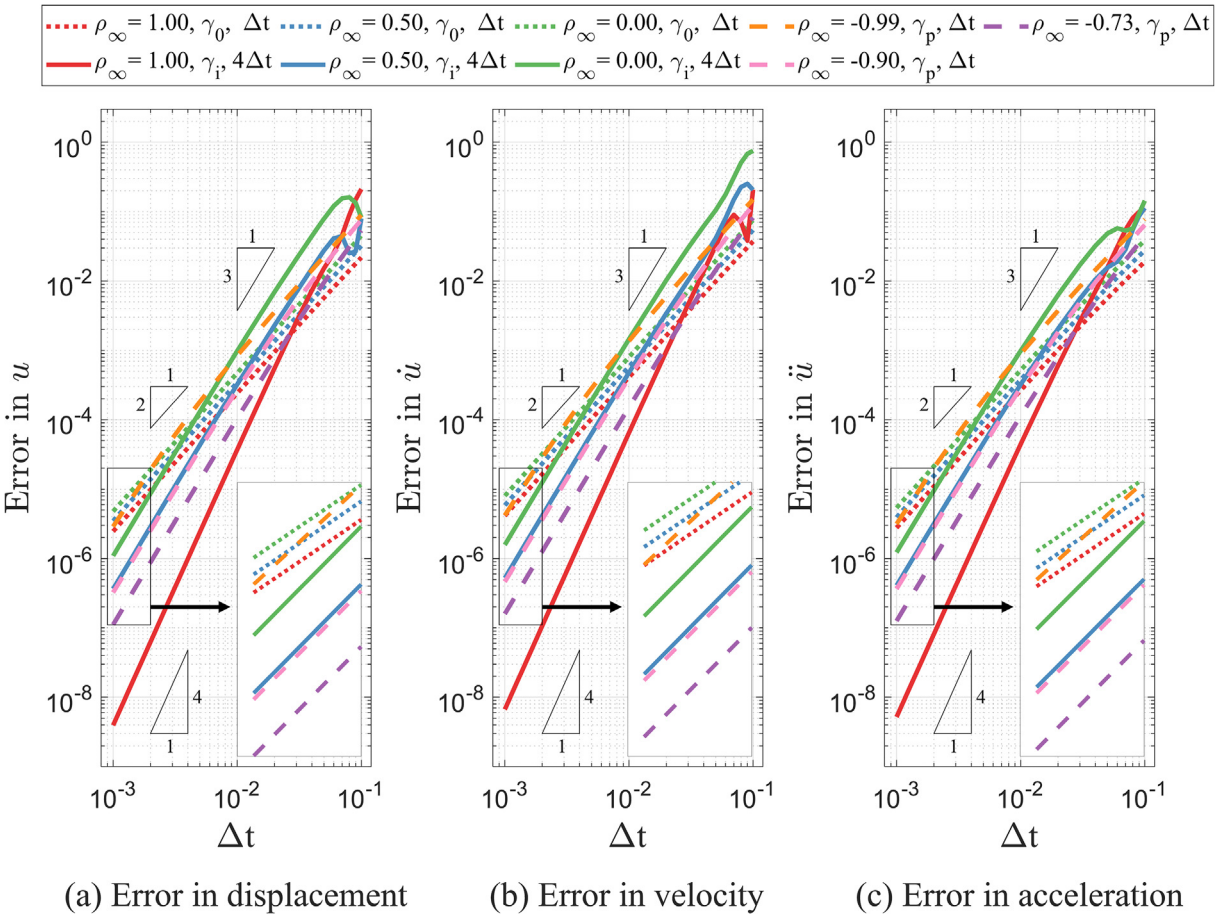

Fig. 10. Damped SDOF system solved using the ρ_∞-Bathe scheme with various values of ρ_∞ and γ.

In this problem we note that using γ_i with $\rho_\infty = 1.0$ provides best performance due to the fourth-order accuracy whereas when using γ_p with $\rho_\infty = 1-\sqrt{3}$ shows best performance and using $\rho_\infty = -0.99$ (here we use $\rho_\infty = (-1, 1-\sqrt{3}]$) shows worst performance (see also Fig. 4).

As expected, with a sufficiently small time step size, the use of γ_p and γ_i gives smaller errors than the use of γ_0 due to the increased order of accuracy.

4.2. A linear three-degree-of-freedom model problem

We revisit here the three-degree-of-freedom model problem which we used to illustrate the performance of time integration schemes when a general structure with stiff and flexible parts is solved (Fig. 11) [28]. Our objective is now to evaluate the effectiveness of using various γ values. We use the lowest possible $|\rho_\infty|$ values for each γ to effectively filter out the high-frequency response; $\rho_\infty = 0$ for γ_0 and γ_i, and $\rho_\infty = 1-\sqrt{3}$ for γ_p.

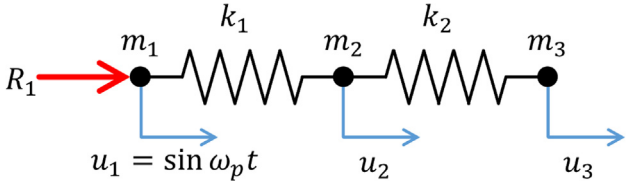

Fig. 11. A stiff-soft spring problem; $k_1 = 10^7$, $k_2 = 1$, $m_1 = 0$, $m_2 = m_3 = 1$, $\omega_p = 1.2$ with zero initial conditions; ${}^0u_2 = {}^0u_3 = {}^0\dot{u}_2 = {}^0\dot{u}_3 = {}^0\ddot{u}_2 = {}^0\ddot{u}_3 = 0$.

Using the standard Bathe method, there is an overshoot in the acceleration at node 2 and in the reaction, but only initially. This overshoot can be eliminated by using a specific set of Newmark parameters, α and δ, only for the first full step [29]. An analytical study shows that using the ρ_∞-Bathe method provides similar behaviors in that the use of $(\alpha, \delta) = ((1+\sqrt{2})/4, (1+\sqrt{2})/2)$, $(3-2\sqrt{3})/4, (2-\sqrt{3})/2)$ and $((5+i\sqrt{2})/12, (5+i\sqrt{2})/6)$ minimizes the overshoots and oscillations during the first few steps, for $(\rho_\infty, \gamma) = (0, \gamma_0)$, $(1-\sqrt{3}\,,\ \gamma_p)$ and $(0\,,\ \gamma_i)$, respectively. We use those parameter sets for the corresponding ρ_∞ and γ values only for the first step.

Figs. 12 and 13 show the results using the ρ_∞-Bathe method with γ_0, γ_p and γ_i and $\Delta t = 0.14$. We also include the results obtained using γ_i with $4\Delta t$.

The use of γ_i with Δt gives the most accurate solution for all solution variables for a long simulation time. Using γ_0, γ_p and γ_i with $4\Delta t$, we still obtain satisfactory results for all solution variables during the early response. However, using γ_i with $4\Delta t$, there is a small phase lag in the predicted acceleration of node 2, but in particular the results are worse at a later time than when using γ_p. Therefore, γ_i would be useful in cases when the time step size must be small, for example, when the largest frequency contained in the external loads is large.

The use of γ_p with $\rho_\infty = 1-\sqrt{3}$ provides the least dispersion error so the most accurate results for the long simulation time. On the other hand, the solution does not contain sufficient numerical dissipation to filter out the high frequency (considered in

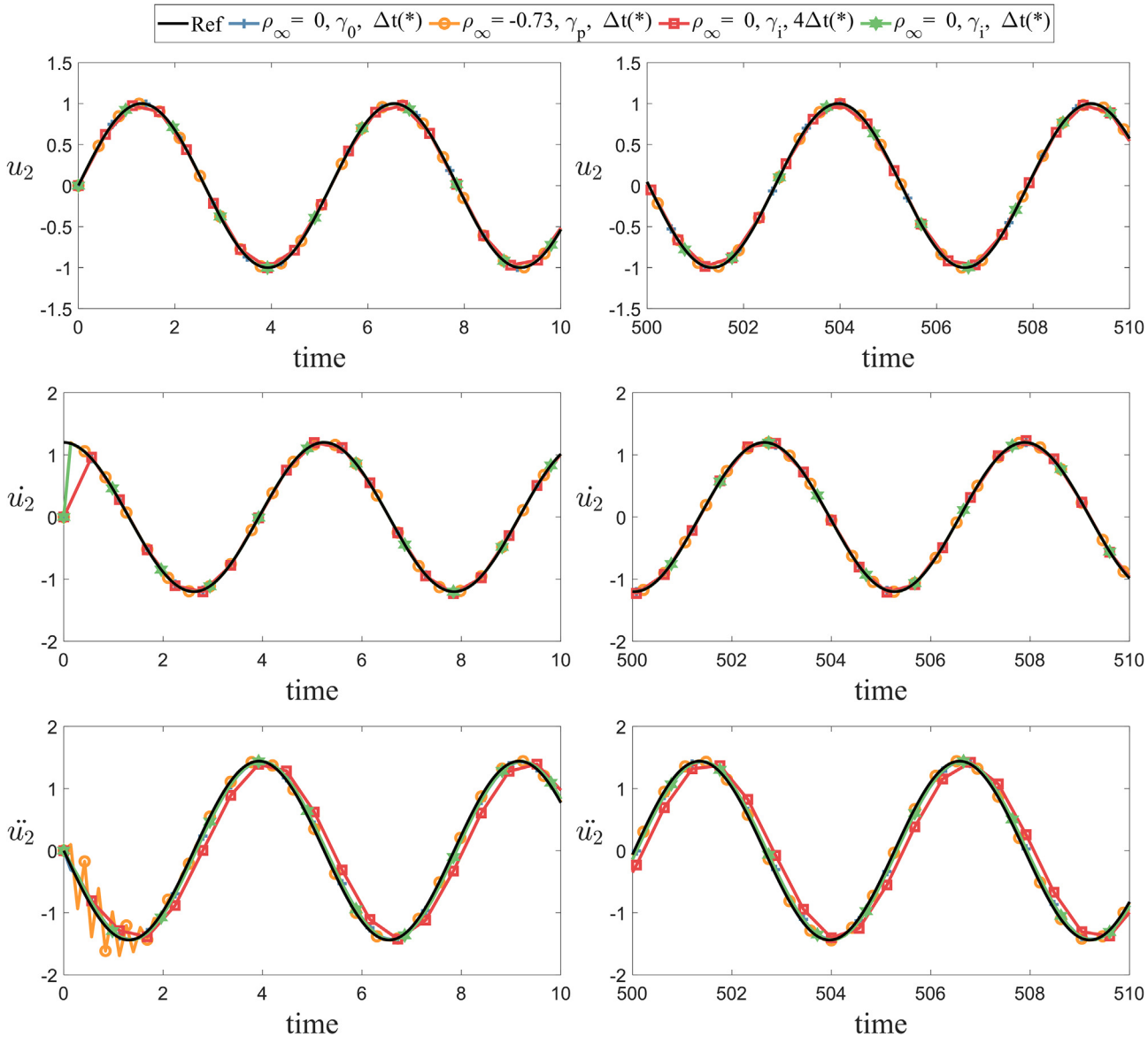

Fig. 12. Predictions of displacement, velocity and acceleration at node 2; "$\rho_\infty = 0,\ \gamma_0,\ \Delta t(*)$" uses $\alpha = (1+\sqrt{2})/4$ and $\delta = (1+\sqrt{2})/2$, "$\rho_\infty = -0.73,\ \gamma_p,\ \Delta t(*)$" uses $\alpha = (3-2\sqrt{3})/4$ and $\delta = (2-\sqrt{3})/2$, "$\rho_\infty = 0,\ \gamma_i,\ \Delta t(*)$" and "$\rho_\infty = 0,\ \gamma_i,\ 4\Delta t(*)$" use $\alpha = (5+i\sqrt{2})/12$ and $\delta = (5+i\sqrt{2})/6$ only for the first step, and $\alpha = 0.25$ and $\delta = 0.5$ otherwise.

practice as spurious [28]) resulting into some oscillations in the first few time steps; therefore, the use of γ_p is preferred when the solutions for a long simulation time are of major interest.

4.3. A nonlinear spring pendulum

We next consider the nonlinear spring pendulum problem shown in Fig. 14 to study the convergence behavior of the method when using various γ values in this problem with geometric nonlinearity. The governing equation and initial conditions are

$$\begin{aligned} &m\ddot{r} + m(L_0 + r)\dot{\theta}^2 - mg\cos(\theta) + kr = 0 \\ &\ddot{\theta} + \tfrac{2\dot{r}\dot{\theta} + g\sin(\theta)}{L_0 + r} = 0 \\ &m = 1, \quad k = 98.1, \quad g = 9.81, \quad L_0 = 0.5 \\ &{}^0r = 0.25\ , \quad {}^0\dot{r} = 0, \quad {}^0\theta = \tfrac{2\pi}{9}, \quad {}^0\dot{\theta} = 0 \end{aligned} \tag{46}$$

where r and θ measure the displacements of the tip mass m in the radial and circumferential directions, respectively, L_0 is the length of the undeformed spring, k is the spring constant, and g is the constant of gravity. The reference solution is obtained using the ρ_∞-Bathe method with $\rho_\infty = 0.999$, γ_i, and $\Delta t = 10^{-7}$.

Figs. 15 and 16 show the error norms of the displacement, velocity, and acceleration in r and θ for various γ values. We observe that γ_0 and γ_p provide second- and third-order accuracy, respectively, and γ_i provides third- and fourth-order accuracy for $\rho_\infty \neq 0.999$ and $= 0.999$, respectively. Note that in the problems having nonlinearity and no modes to filter out, we frequently use ρ_∞ slightly less than 1.0 to avoid possible numerical instability. The numerical results show that using γ_i with ρ_∞ values slightly less than 1.0 still provides fourth-order accuracy.

In the use of γ_p, as in the linear SDOF example in Section 4.1, the smallest value of $|\rho_\infty|$, $\rho_\infty = 1 - \sqrt{3}$, provides the best solutions due to minimized period elongations. Also, we observe that the solutions using γ_p with $\rho_\infty > 0.9$ tend to diverge in this nonlinear analysis.

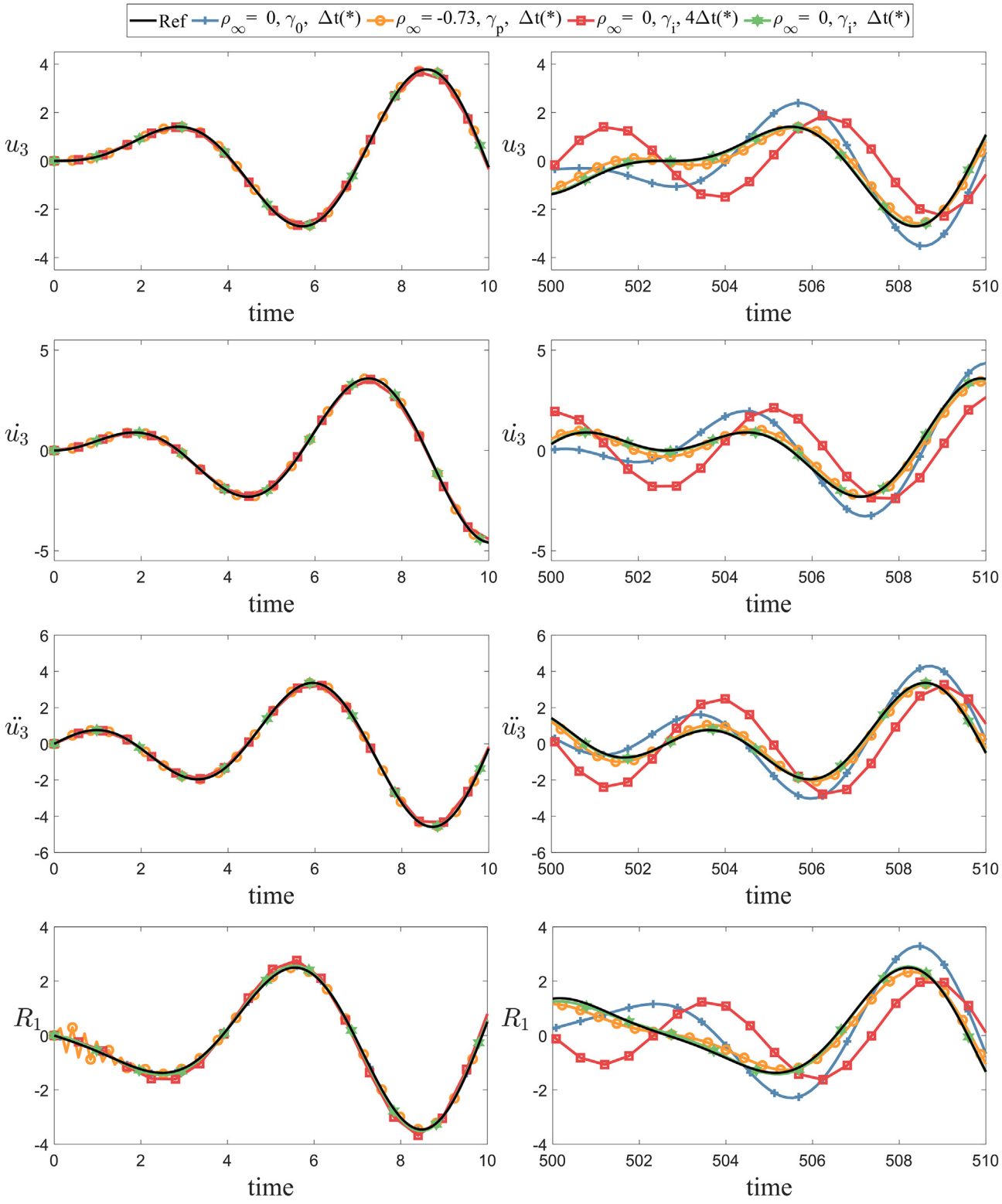

Fig. 13. Predictions of displacement, velocity and acceleration at node 3 and reaction force; "$\rho_\infty = 0,\ \gamma_0,\ \Delta t(*)$" uses $\alpha = (1+\sqrt{2})/4$ and $\delta = (1+\sqrt{2})/2$, "$\rho_\infty = -0.73,\ \gamma_p,\ \Delta t(*)$" uses $\alpha = (3-2\sqrt{3})/4$ and $\delta = (2-\sqrt{3})/2$, "$\rho_\infty = 0,\ \gamma_i,\ \Delta t(*)$" and "$\rho_\infty = 0,\ \gamma_i,\ 4\Delta t(*)$" use $\alpha = (5+i\sqrt{2})/12$ and $\delta = (5+i\sqrt{2})/6$ only for the first step, and $\alpha = 0.25$ and $\delta = 0.5$ otherwise.

Fig. 17 shows the errors in r and θ using various values of γ with $\Delta t = 10^{-3}$. This analysis illustrates that the use of γ_p and γ_i is more effective than using γ_o in the solution of some problems.

4.4. A single-degree-of-freedom parabolic system

We first consider a typical linear single-degree-of-freedom parabolic system, $\dot{T} + T = 0$, with the initial conditions of

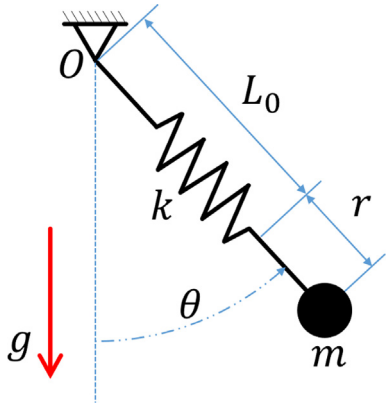

Fig. 14. A nonlinear spring pendulum.

${}^0T = 100$ and ${}^0\dot{T} = -100$, respectively. To illustrate the order of accuracy of the ρ_∞-Bathe method with γ_0, γ_p and γ_i for a parabolic system, we use the error norms defined in Eq. (45) where the exact temperature solution is $T = 100e^{-t}$.

Fig. 18 shows the error norms calculated using the solutions from 0 s to 10 s. As in structural dynamics, γ_0 and γ_p provide second- and third-order accuracy, respectively, and γ_i provides third- and fourth-order accuracy for $\rho_\infty \neq 1$ and $= 1$, respectively.

In heat transfer analysis we can encounter undesired oscillations in the predicted response when the exact response changes rapidly compared to the considered time step size. To illustrate the performance of the schemes in such situations, we consider the same model solved above using very large time step sizes. Figs. 19 and 20 show the results of T and $\dot{T}$ calculated using the ρ_∞-Bathe method with various ρ_∞ and γ values and the α-method with $\alpha = 0.5$ [3]. For all considered time step sizes, the α-method with $\alpha = 0.5$ and the ρ_∞-Bathe method $\rho_\infty = 1 - \sqrt{3}$ with γ_p give large oscillations while using the ρ_∞-Bathe method with $\rho_\infty = 0$ and γ_0 and γ_i provides satisfactory results. Therefore, as in the solution of structural dynamics problems (see Section 4.2), the use of $\rho_\infty = 0$ is valuable when a general finite element system including parts with largely different heat conductivities is solved.

4.5. A two- degree-of-freedom parabolic system with large difference in conductivities

Next, we consider a linear two-degree-of-freedom parabolic system with "stiff and soft parts" [30]. The governing equation and initial conditions are

$$\begin{Bmatrix} \dot{T}_1 \\ \dot{T}_2 \end{Bmatrix} = \begin{bmatrix} 998 & 1998 \\ -999 & -1999 \end{bmatrix} \begin{Bmatrix} T_1 \\ T_2 \end{Bmatrix} \tag{47}$$

$${}^0T_1 = 1 \quad {}^0T_2 = 0$$

$${}^0\dot{T}_1 = 998 \quad {}^0\dot{T}_2 = -999$$

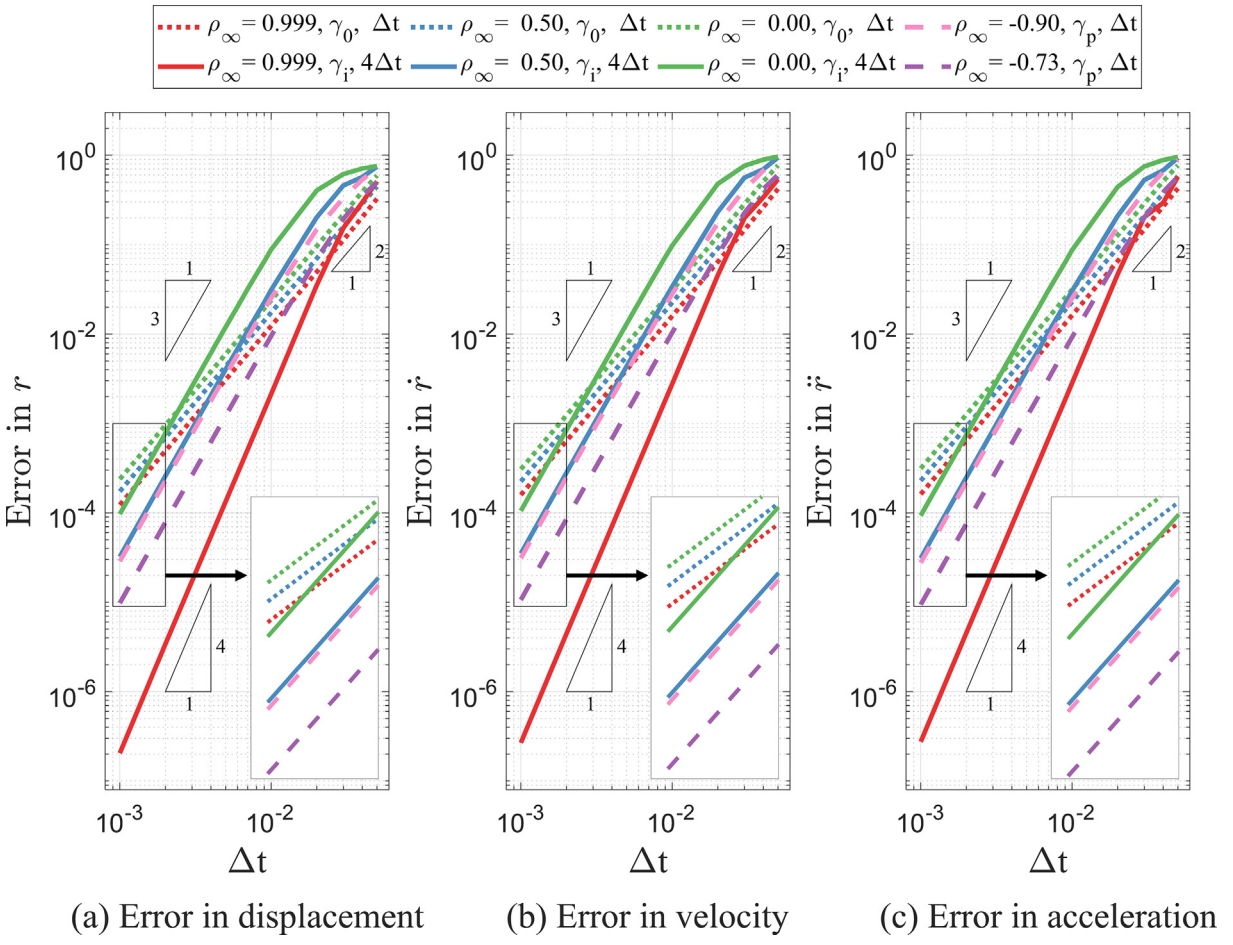

Fig. 15. A nonlinear spring pendulum, r is measured.

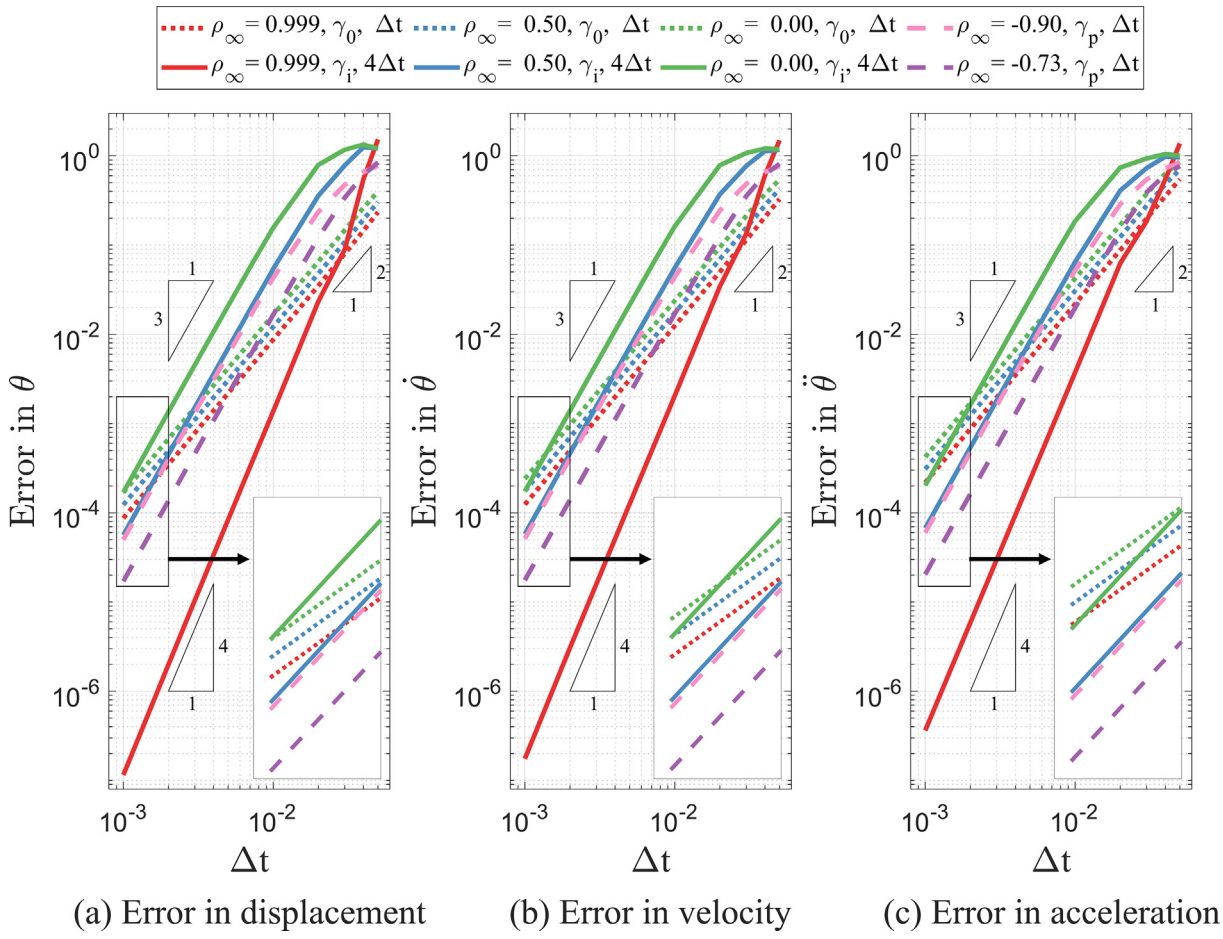

Fig. 16. A nonlinear spring pendulum, θ is measured.

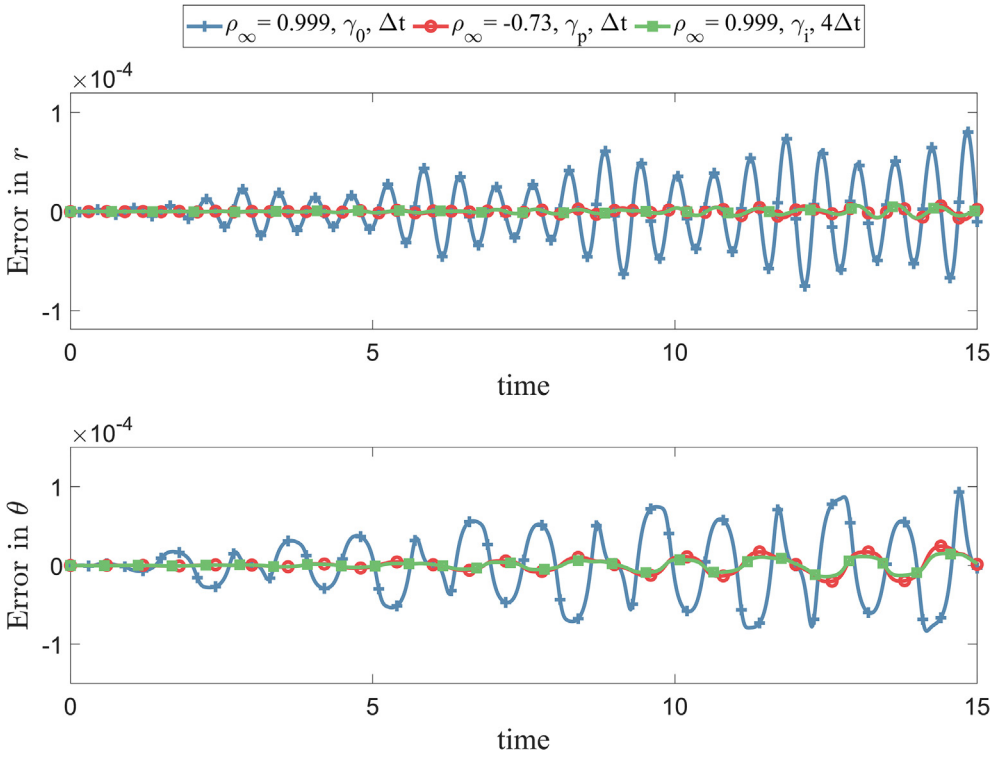

Fig. 17. Errors in r and θ obtained when using γ_0, γ_p and γ_i.

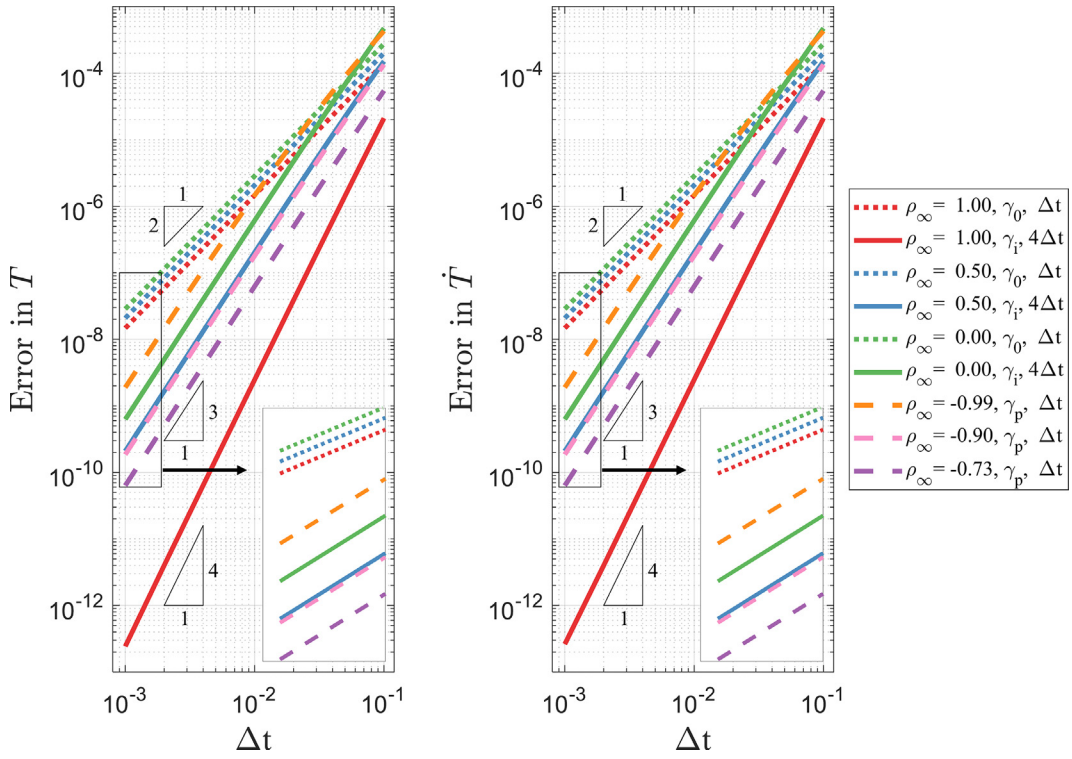

Fig. 18. Errors in solution of a linear single-degree-of-freedom parabolic system, T denotes temperature.

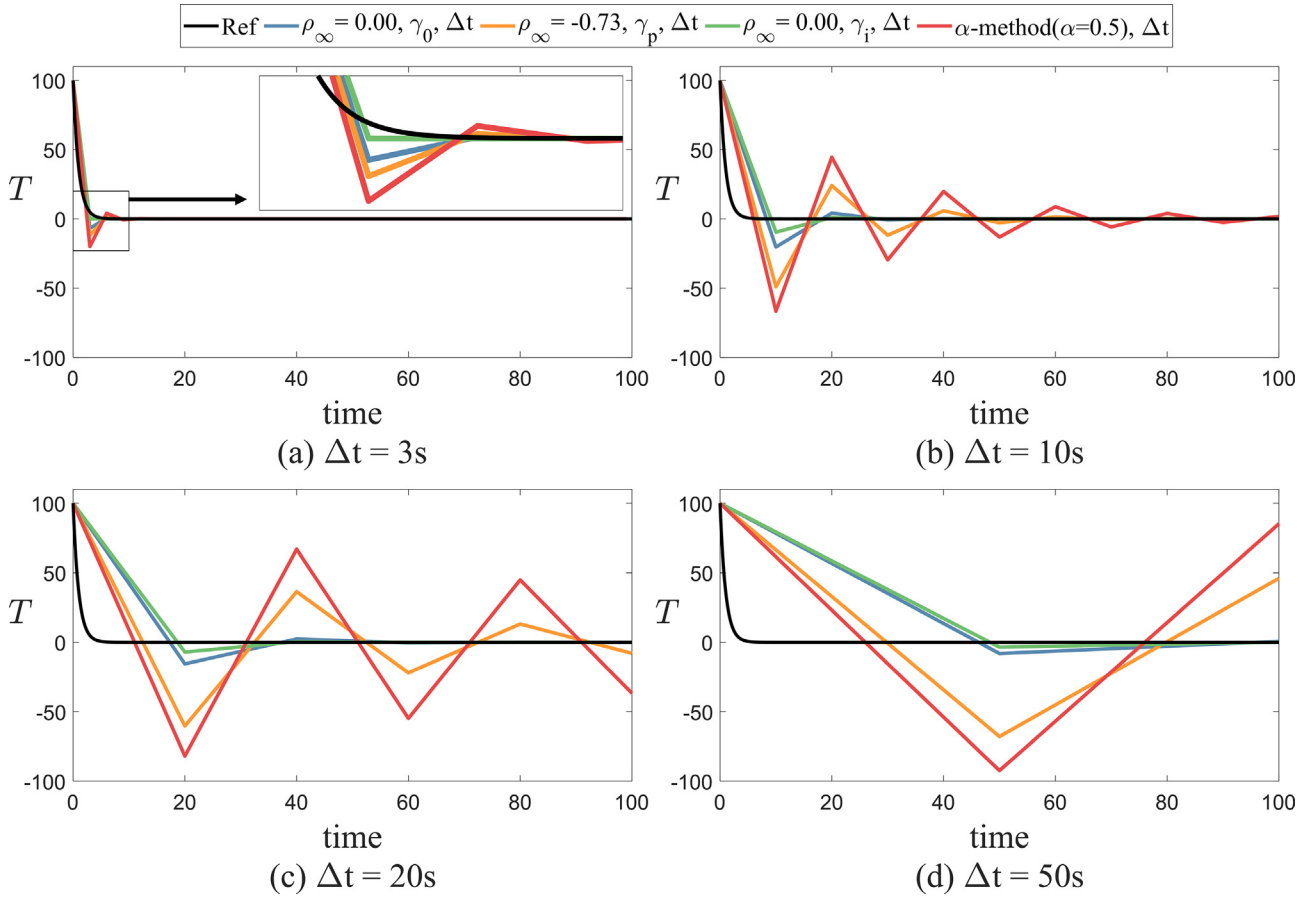

Fig. 19. Predicted temperature T of a linear single-degree-of-freedom parabolic system with various time steps, $\Delta t = 3,\ 10,\ 20,\ 50s$; The governing equation is $\dot{T} + T = 0$ with the initial conditions ${}^0T = 100$ and ${}^0\dot{T} = -100$.

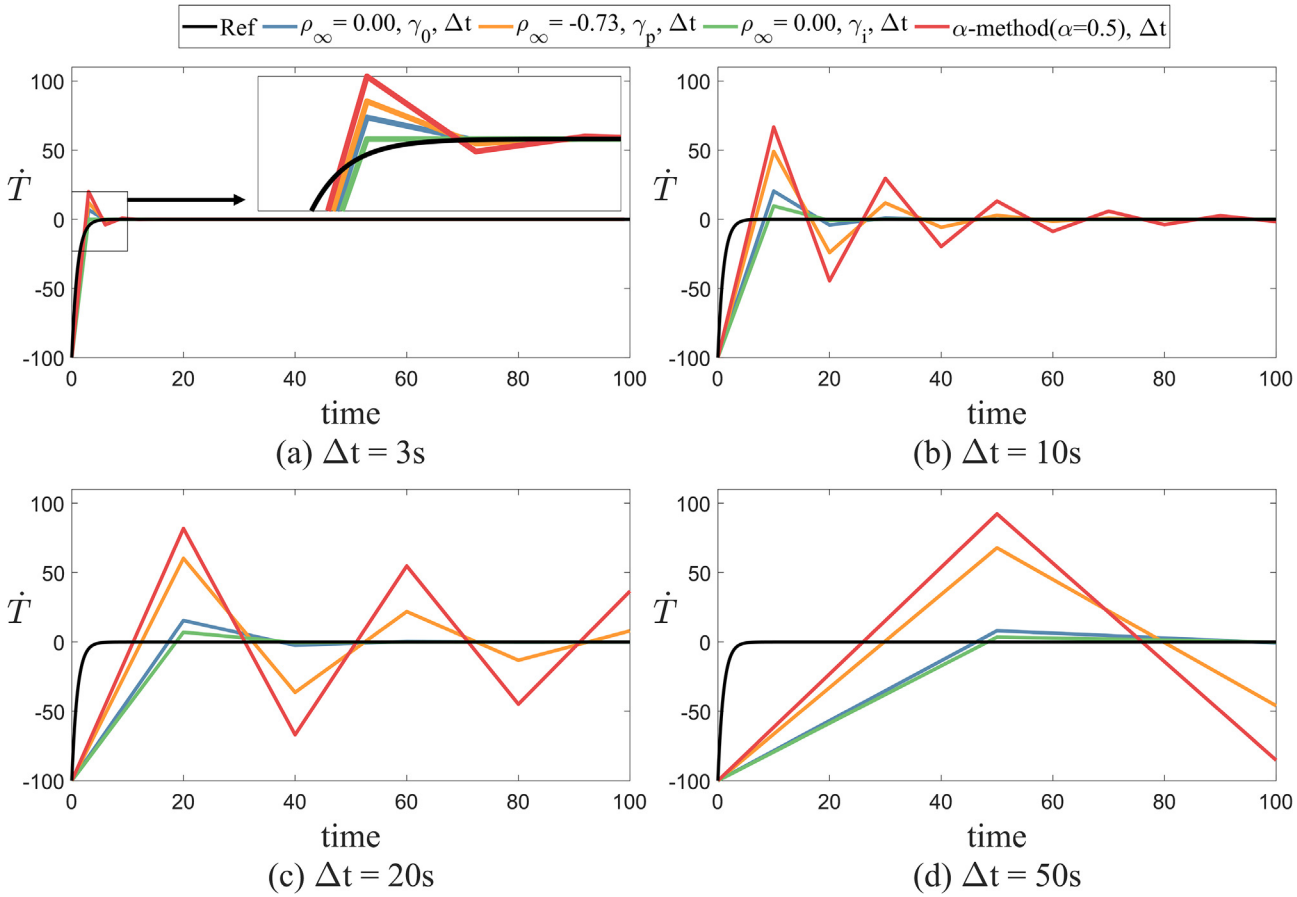

Fig. 20. Predicted temperature change $\dot{T}$ of a linear single-degree-of-freedom parabolic system with various time steps, $\Delta t = 3,\ 10,\ 20,\ 50s$; The governing equation is $\dot{T} + T = 0$ with the initial conditions ${}^0T = 100$ and ${}^0\dot{T} = -100$.

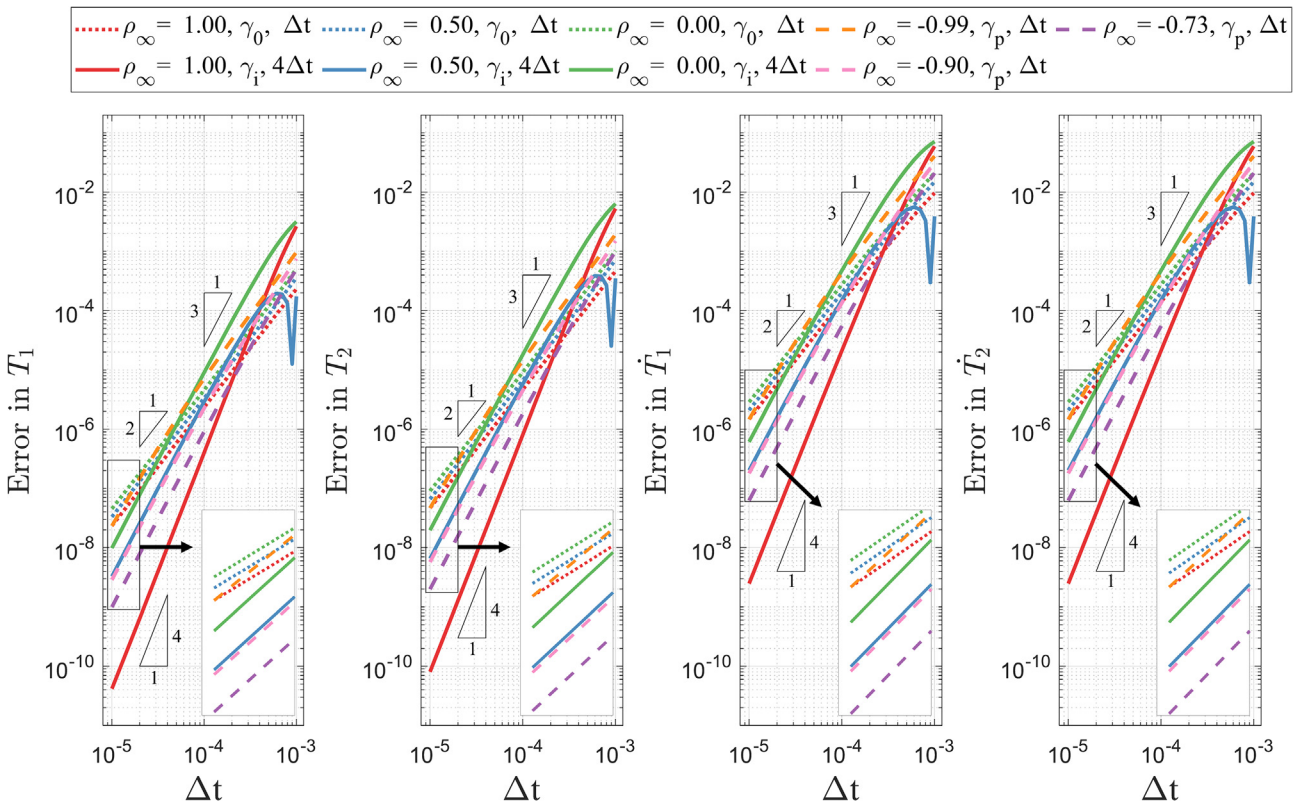

Fig. 21. Errors in solution of a linear two-degree-of-freedom parabolic system, T denotes temperature.

for which the exact solution is $T_1 = 2e^{-t} - e^{-1000t}$ and $T_2 = e^{-t} + e^{-1000t}$.

Fig. 21 shows the error norms calculated using Eq. (45) for the response from 0 to 5 s.

As in the solution of the SDOF system, we observe the expected order of accuracy for each pair of γ and ρ_∞ values in all solution variables.

4.6. A two-dimensional heat conduction system

Lastly, we consider a two-dimensional heat conduction system [36]. The governing equation, boundary and initial conditions are

$$\begin{aligned} &k\Delta^2 T = \tfrac{\partial T}{\partial t} \\ &T(0,y,t) = T(x,0,t) = T(L_x,y,t) = T(x,L_y,t) = 0 \\ &T(x,y,0) = 30 \end{aligned} \tag{48}$$

where k is the thermal diffusivity, L_x and L_y are the lengths of the solution domain in the x and y directions, respectively. The analytical solution is given as [36]

$$T(x,y,t) = \sum_{n=1}^{\infty}\sum_{m=1}^{\infty} A_n \sin\frac{n\pi x}{L_x}\sin\frac{m\pi y}{L_y} \times \exp\left[-\left(\frac{kn^2\pi^2}{L_x^2} + \frac{km^2\pi^2}{L_y^2}\right)t\right] \tag{49}$$

where

$$A_n = \frac{120}{nm\pi^2}[(-1)^n - 1][(-1)^m - 1] \tag{50}$$

The errors in the temperature at $t = 15s$ are show in Fig. 22. As in the results of the SDOF system in Section 4.4, using the ρ_∞-Bathe method with ρ_∞ = 0 and γ_0 or γ_i provides satisfactory results, even with the very large time step sizes.

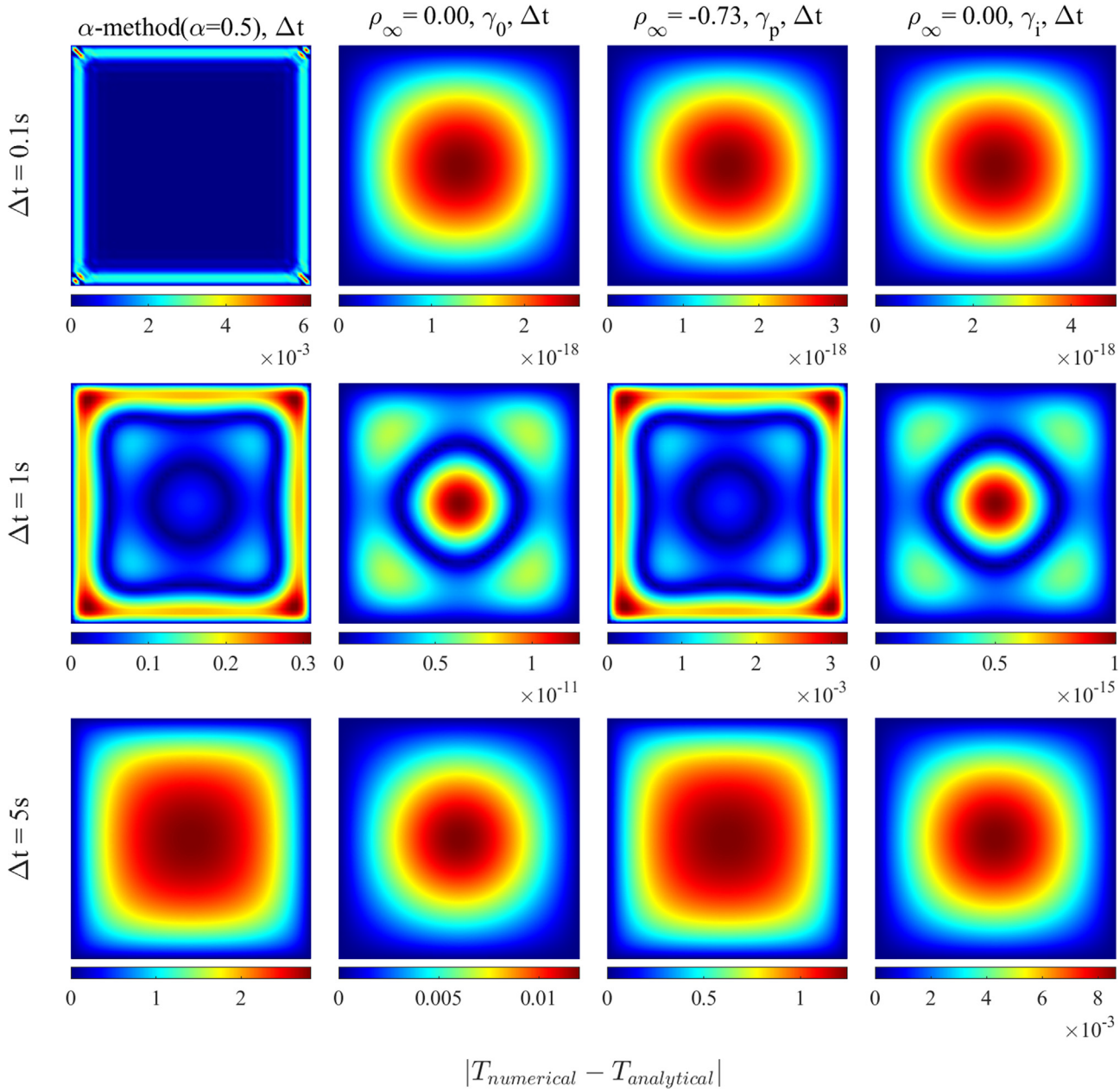

Fig. 22. Errors in temperature with various time steps; The solution domain is $[0,3] \times [0,3]$; The thermal diffusivity $k = 1.25$.

5. Concluding remarks

We considered in this paper the splitting ratio of the ρ_∞-Bathe method to increase the order of accuracy of the solutions obtained in finite element analyses of structural dynamics and heat transfer.

For both types of analyses, we identified three useful γ values and their corresponding ρ_∞ ranges: γ_0 with $\rho_\infty \in [0,1]$ and γ_p with $\rho_\infty = (-1, 1-\sqrt{3}]$ which provide second- and third-order accuracy, respectively, and γ_i with $\rho_\infty \in [0,1]$ which provides third-order accuracy except when ρ_∞ is very close to 1 where the use results in fourth-order accuracy. The use of γ_p does not increase the computational cost compared to the use of γ_o while the possible range of $|\rho_\infty|$ is reduced to $|\rho_\infty| \in [\sqrt{3}-1, 1)$. On the other hand, γ_i can be used with $\rho_\infty \in [0,1]$ but being a complex number, the use of γ_i requires a larger computational effort than the use of γ_o or γ_p when employing the same time step size Δt, and also significantly more memory.

We illustrated the findings of our theoretical study in example solutions and observed the expected order of accuracy in all solution variables. The ρ_∞-Bathe method with γ_o provided sufficiently accurate solutions in all considered structural dynamics and heat transfer analyses. The use of γ_p with $\rho_\infty = 1-\sqrt{3}$ provided notably enhanced solutions for relatively long simulation times without additional computational cost. On the other hand, due to the possible range $|\rho_\infty| \in [\sqrt{3}-1, 1)$, we may have some oscillations in the initial time steps when the problem includes spurious modes to be filtered out. The use of γ_i can be useful in practice when there is no spurious mode and the time step needs to be small.

In the use of γ_i, while we have real-valued solutions at the full time steps, $t+\Delta t$, we have complex-valued solutions at the intermediate time points, $t+\gamma_i \Delta t$. These complex values can be regarded as numerically useful to improve the physically meaningful solutions at the required times but special solvers of the resulting equations should be developed to optimize the solution time and memory used.

In this paper, we focused on the time splitting ratio to achieve higher-order accuracy in the ρ_∞-Bathe method. Further studies are needed to investigate the optimal use of the parameters of the ρ_∞-Bathe method with modern spatial discretizations, including overlapping finite elements [31–33], in particular for the analysis of wave propagations [34,35]. Also, studies focusing on the optimal load to be used at the intermediate time point for various splitting values would be very valuable, and schemes for adaptive time stepping using the Bathe methods may be effective.

Declaration of Competing Interest

The authors declare that they have no known competing financial interests or personal relationships that could have appeared to influence the work reported in this paper.

Acknowledgment

This work was partly supported by the Young Scientist Grants-Outstanding Track (Grant No. NRF-2021R1C1C1011494) through the National Research Foundation of Korea (NRF) funded by the Ministry of Science and ICT.

Appendix

$$\begin{bmatrix} \dot{x}_{t+\Delta t} \\ x_{t+\Delta t} \end{bmatrix} = \boldsymbol{A}_{\text{exact}} \begin{bmatrix} \dot{x}_t \\ {}^t x \end{bmatrix}$$

$$\boldsymbol{A}_{\text{numerical}} = \frac{1}{\beta_1}\begin{bmatrix} a_{11} & a_{12} \\ a_{21} & a_{22} \end{bmatrix}$$

where

$$\begin{aligned}\beta_1 &= (\gamma^2\Omega^2 + 4\gamma\xi\Omega + 4)((\Omega^2 - 2\xi(\rho_\infty - 1)\Omega + (\rho_\infty - 1)^2)\gamma^2 \\ &\quad + (-2\Omega^2 + 2\xi(\rho_\infty - 3)\Omega + 4(\rho_\infty - 1))\gamma + \Omega^2 + 4\xi\Omega + 4)\end{aligned}$$

$$\begin{aligned}a_{11} &= (\rho_\infty\Omega^2 - 2\rho_\infty\xi(\rho_\infty - 1)\Omega + (\rho_\infty - 1)^2)\gamma^4\Omega^2 - (2\rho_\infty\Omega^3 \\ &\quad - 2\xi\rho_\infty(\rho_\infty - 1)\Omega^2 + 4(2\rho_\infty\xi^2 - 1)(\rho_\infty - 1)\Omega \\ &\quad - 4\xi(\rho_\infty - 1)^2)\gamma^3\Omega + (\rho_\infty\Omega^4 - 4\xi\rho_\infty\Omega^3 - 2(\rho_\infty - 3)(1 \\ &\quad - 4\rho_\infty\xi^2 + \rho_\infty)\Omega^2 - 8\xi(\rho_\infty - 1)(\rho_\infty - 2)\Omega + 4(\rho_\infty - 1)^2)\gamma^2 \\ &\quad + (4\xi\rho_\infty\Omega^3 + 8(2\xi^2 - 1)\rho_\infty\Omega^2 - 24\xi(\rho_\infty - 1)\Omega + 16\rho_\infty \\ &\quad - 16)\gamma - 4\Omega^2 - 16\xi\Omega + 16\end{aligned}$$

$$\begin{aligned}a_{12} &= -\omega\Big(16 + (\rho_\infty - 1)^2\gamma^4\Omega^2 \\ &\quad - ((\rho_\infty - 3)\Omega - 4\xi(\rho_\infty - 1))(\rho_\infty - 1)\gamma^3\Omega \\ &\quad + (4\Omega^2 - 4\xi(\rho_\infty - 1)(\rho_\infty - 3)\Omega + 4(\rho_\infty - 1)^2)\gamma^2 \\ &\quad + \Big(-2(\rho_\infty + 1)\Omega^2 - 8\xi(\rho_\infty - 1)\Omega + 16\rho_\infty - 16\Big)\gamma\Big)\Omega\end{aligned}$$

$$\begin{aligned}a_{21} &= \Big(16 + (\rho_\infty - 1)^2\gamma^4\Omega^2 - ((\rho_\infty - 3)\Omega \\ &\quad - 4\xi(\rho_\infty - 1))(\rho_\infty - 1)\gamma^3\Omega + (4\Omega^2 - 4\xi(\rho_\infty - 1)(\rho_\infty - 3)\Omega \\ &\quad + 4(\rho_\infty - 1)^2)\gamma^2 + (-2(\rho_\infty + 1)\Omega^2 \\ &\quad - 8\xi(\rho_\infty - 1)\Omega + 16\rho_\infty - 16)\gamma\Big)\Delta t\end{aligned}$$

$$\begin{aligned}a_{22} &= (\rho_\infty\Omega^2 - 2\xi(\rho_\infty - 1)\Omega + (\rho_\infty - 1)^2)\gamma^4\Omega^2(2\rho_\infty\Omega^3 - 6\xi(\rho_\infty - 1)\Omega^2 \\ &\quad + 4(2\xi^2 - 1)(\rho_\infty - 1)\Omega - 4\xi(\rho_\infty - 1)^2)\gamma^3\Omega \\ &\quad + (\Omega^4\rho_\infty - 4\xi(\rho_\infty - 2)\Omega^3 + 2(\rho_\infty - 3)(4\xi^2 - \rho_\infty - 1)\Omega^2 \\ &\quad + 8\xi(\rho_\infty - 1)\Omega + 4(\rho_\infty - 1)^2)\gamma^2 + (-4\xi\Omega^3 + 8(2\xi^2 - \rho_\infty)\Omega^2 \\ &\quad + 8\xi(\rho_\infty - 1)\Omega + 16\rho_\infty - 16)\gamma - 4\Omega^2 + 16\xi\Omega + 16\end{aligned}$$

References

[1] Bathe KJ. The finite element method. In: Linderberg T, Wah B, editors. Encyclopedia of computer science and engineering. Hoboken, New Jersey: J. Wiley and Sons; 2009. p. 1253–64.
[2] Bathe KJ. Frontiers in finite element procedures & applications. In: Topping BHV, Iványi P, editors. Chapter 1 in computational methods for engineering technology. Stirlingshire, Scotland: Saxe-Coburg Publications; 2014.
[3] Bathe KJ. Finite element procedures, 2nd ed. In: Bathe KJ, editor. Watertown, MA; also published by Higher Education Press China; 2016.
[4] Newmark NM. A method of computation for structural dynamics. J Eng Mech Divs 1959;85(3):67–94.
[5] Wilson EL, Farhoomand I, Bathe KJ. Nonlinear dynamic analysis of complex structures. Int J Earthq Eng Struct Dyn 1973;1:241–52.
[6] Hilber HM, Hughes TJR, Taylor RL. Improved numerical dissipation for time integration algorithms in structural dynamics. Earthq Eng Struct Dyn 1977;5(3):283–92.
[7] Wood WL, Bossak M, Zienkiewicz OC. An alpha modification of Newmark's method. Int J Numer Methods Eng 1980;15(10):1562–6.
[8] Shao HP, Cai CW. A three parameters algorithms for numerical integration of structural dynamic equations. Chin J Appl Mech 1988;5(4):76–81.
[9] Chung J, Hulbert GM. A time integration algorithm for structural dynamics with improved numerical dissipation: the generalized-alpha method. J Appl Mech (ASME) 1993;60(2):371–5.
[10] Tamma KK, Zhou X, Sha D. The time dimension: A theory towards the evolution, classification, characterization and design of computational algorithms for transient/dynamic applications. Arch Comput Methods Eng 2000;7(2):67–290.
[11] Bathe KJ, Baig MMI. On a composite implicit time integration procedure for nonlinear dynamics. Comput Struct 2005;83(31–32):2513–4.
[12] Bathe KJ. Conserving energy and momentum in nonlinear dynamics: a simple implicit time integration scheme. Comput Struct 2007;85(7–8):437–45.
[13] Noh G, Bathe KJ. An explicit time integration scheme for the analysis of wave propagations. Comput Struct 2013;129:178–93.

[14] Wen WB, Wei K, Lei HS, Duan SY, Fang DN. A novel sub-step composite implicit time integration scheme for structural dynamics. Comput Struct 2017;182:176–86.
[15] Kim W, Choi SY. An improved implicit time integration algorithm: The generalized composite time integration algorithm. Comput Struct 2018;196:341–54.
[16] Zhang HM, Xing YF. Optimization of a class of composite method for structural dynamics. Comput Struct 2018;202:60–73.
[17] Malakiyeh MM, Shojaee S, Bathe KJ. The Bathe time integration method revisited for prescribing desired numerical dissipation. Comput Struct 2019;212:289–98.
[18] Li J, Yu K, Li X. A novel family of controllably dissipative composite integration algorithms for structural dynamic analysis. Nonlinear Dyn 2019;96 (4):2475–507.
[19] Ji Y, Xing YF. An optimized three-sub-step composite time integration method with controllable numerical dissipation. Comput Struct 2020;231:106210.
[20] Li J, Yu K. A novel family of composite sub-step algorithms with desired numerical dissipations for structural dynamics. Arch Appl Mech 2020;90 (4):737–72.
[21] Zhang H, Zhang R, Xing Y, Masarati P. On the optimization of n-sub-step composite time integration methods. Nonlinear Dyn 2020;102(3):1939–62.
[22] Wen W, Deng S, Wang N, Duan S, Fang D. An improved sub-step time-marching procedure for linear and nonlinear dynamics with high-order accuracy and high-efficient energy conservation. Appl Math Model 2021;90:78–100.
[23] Malakiyeh MM, Shojaee S, Hamzehei-Javaran S, Bathe KJ. New insights into the β_1/β_2-Bathe time integration scheme when L-stable. Comput Struct 2021;245:106433.
[24] Noh G, Bathe KJ. The Bathe time integration method with controllable spectral radius: the ρ_∞-Bathe method. Comput Struct 2019;212:299–310.
[25] Noh G, Bathe KJ. For direct time integrations: A comparison of the Newmark and ρ_∞-Bathe schemes. Comput Struct 2019;225:106079.
[26] Kwon S-B, Bathe KJ, Noh G. Selecting the load at the intermediate time point of the ρ_∞-Bathe time integration scheme. Comput Struct 2021;254:106559.
[27] Kwon S-B, Bathe KJ, Noh G. An analysis of implicit time integration schemes for wave propagations. Comput Struct 2020;230:106188.
[28] Bathe KJ, Noh G. Insight into an implicit time integration scheme for structural dynamics. Comput Struct 2012;98:1–6.
[29] Noh G, Bathe KJ. Further insights into an implicit time integration scheme for structural dynamics. Comput Struct 2018;202:15–24.
[30] Gear CW. Numerical initial value problems in ordinary differential equations. Prentice Hall; 1971.
[31] Bathe KJ. The AMORE paradigm for finite element analysis. Adv Eng Softw 2019;130:1–13.
[32] Chai Y, Bathe KJ. Transient wave propagation in inhomogeneous media with enriched overlapping triangular elements. Comput Struct 2020;237:106273.
[33] Lee S, Bathe KJ. An enhancement of overlapping finite elements. Comput Struct 2022;260:106704.
[34] Noh G, Ham S, Bathe KJ. Performance of an implicit time integration scheme in the analysis of wave propagations. Comput Struct 2013;123:93–105.
[35] Zakian P, Bathe KJ. Transient wave propagations with the Noh-Bathe scheme and the spectral element method. Comput Struct 2021;254:106531.
[36] Bruch Jr JC, Zyvoloski G. Transient two-dimensional heat conduction problems solved by the finite element method. Int J Numer Methods Eng 1974;8 (3):481–94.